Thesis for the M. S. Degree

Segmentation of SAR Sea Ice Imagery using Local Fractal Dimension

국소 프랙탈 차원을 이용한 합성개구레이더 해빙 영상의 분할기법 연구

2014 년 7 월

서울대학교 대학원

지구환경과학부

임 성 재

Segmentation of Sea Ice SAR Images using Local Fractal Dimension

국소 프랙탈 차원을 이용한 합성개구레이더 해빙 영상의 분할기법 연구

지도 교수 김 덕 진

이 논문을 이학석사 학위논문으로 제출함

2014 년 4 월

서울대학교 대학원
지구환경과학부
임 성 재

임성재의 이학석사 학위논문을 인준함
2014 년 7 월

위 원 장 이 준 기 (인)

부위원장 김 덕 진 (인)

위 원 박 상 은 (인)

Abstract

The climate change is a popular issue. People usually regard the concept of climate change as an image of polar bear on the melting sea ice. The climate has really been changed and it possibly causes disasters without warning. Make it worse, the scale and frequency of disasters has been increased. To predict and prepare future climate, many researches have investigated the climate system. A computer simulation is a useful tool for this research. The goal of simulation is to know more reliable future climate trend from many climate parameters. In this manner, recent climate models include the properties of sea ice, because the sea ice is closely connected with the global energy budget of the Earth and the circulation of the ocean and atmosphere.

In fact, the sea ice an essential factor in the polar climate investigation. First of all, the sea ice and snow on surface has a high albedo. Most solar radiation energy are reflected on sea ice surface. Otherwise, the open water region has low albedo and absorbs more solar energy. In this manner, the albedo of sea ice controls the energy budget of polar region. Secondly, the sea ice acts as an insulator between the ocean and the atmosphere. In this case, the thicker sea ice is, the better insulator. Thick sea ice effectively prohibits a heat exchange between the ocean and the atmosphere. Thus the circulation of the ocean and the atmospheric are affected. Third, the sea ice controls the salinity of the ocean. Sea ice contains a salinity as a small droplet called the brine cell. It is slightly going down by its high salinity when time goes by. This falling process ends up when the salinity enters to the ocean. On the other hand, a fresh water is added into the ocean when the melting process of sea ice is occurred without brine cells. By these means, the salinity of the ocean is affected by the sea ice. Consequently, the sea ice executes important roles for the polar climate and global climate system. In this manner, measuring properties of the sea ice is important for reasonable

climate system simulation. This modeling process is closely connected with the climate change prediction.

For decades, many satellite missions have been operated for monitoring the sea ice region. The Synthetic Aperture Radar (SAR) system has been included among these observations. The SAR has good characteristics on the polar region observation. The SAR system is rarely affected by the atmospheric or weather condition. This feature can be archived by using the microwave frequency. The microwave band is located in the atmospheric window. It does not absorbed by particles in atmosphere likewise water vapor or ozone. Another advantage of the SAR mission is a wide swath. SAR system could monitor the wide area in one observation process. The other characteristics of SAR system is an active sensor. The active means that it can radiate and receive the signal. Thus SAR system can be operated in night time without sun light. In addition, it can make clear image by controlling strength of the signal. With these advantages, the SAR system is suitable for monitoring the polar region.

Due to these observations, a lot of sea ice data has been accumulated in present. The data should be operated for extracting the parameters what we need. In this study, I want to make parameters by segmentation technique. The segmentation of sea ice has still been remained a challengeable task. The difficulty of sea ice segmentation is connected to the scattering mechanism of the sea ice in electromagnetic radiation. In the view of the microwave sensor, the sea ice surface is rough, so sea ice is represented as a heterogeneous bulk region in SAR images. In addition, the speckle noise in SAR images makes it worse the sea ice segmentation. I focused on these characteristics and tried to parameterize this feature.

The Fractal Geometry was introduced by Mandelbrot. It can measure the randomness in the nature or self-similarity. The Local Fractal Dimension (LFD) can determine heterogeneity of the sea ice region by fractal geometry. For this reason, the LFD was adopted in the segmentation process in this

study. After the LFD calculation, the sea ice pixels have high LFD value; otherwise the open water pixels have relatively low LFD value. With LFD calculation, pixels were separated by sea ice and open water. In this manner, the LFD is shown a useful tool for segmentation purpose.

In addition, the Markov Random Field (MRF) segmentation method was also utilized in this study. The MRF segmentation method is based on a probability model and uses statistical parameters of input image. MRF segmentation method uses two aspect of image. One is feature energy and another is label energy. Conventionally, the feature energy has been measured by the Gaussian maximum likelihood function. It assume that the pixels in image are followed the Gaussian distribution. By this means, the feature energy determines a similarity of initial classes and interested pixel. MRF segmentation also uses the clique potential to establish the label energy. It describes a relationship between adjacent pixels in local region. These two aspects of the image establish the cost function of the MRF segmentation. With cost function, the segmentation task is same as an optimization process. To resolve this, the MRF segmentation method has used the Expectation-Maximization (EM) algorithm in operation.

The proposed segmentation method is composed following two phases. First, the LFD of input SAR image was derived. In second phase, the LFD image was inserted to the MRF segmentation method. For comparing reason, a hybrid image was made by original SAR image and calculated LFD image. The segmentation results were resembled in both LFD input and hybrid input cases. Though, segmentation results from hybrid images were shown more similar to human interpretation. These segmentation results were evaluated by an unsupervised evaluation method for segmentation. This method uses inter-class disparity and intra-class disparity for making criterion values.

In this study, the TerraSAR-X images are used for testing the proposed segmentation method. The SAR images are taken in the Arctic sea in

summer season. In the summer season, sea ice suffers melting process. So the shape of sea ice is irregular and chaotic. Even though, the proposed method could produce successful segmentation results from these SAR images. And successful segmentation results are could be converted to the ice concentration rate in that region. This calculation also performed in present study. For guarantee the result of ice concentration, ice concentration data from the Advanced Microwave Scanning Radiometer - Earth Observing System (AMSR-E) and aerial photographs were used in this study.

The result of this study shows that the proposed segmentation method could provide advanced segmentation results. The LFD could capture the characteristics of sea ice and separate sea ice and open water pixels in SAR images. Especially, the segmentation results from hybrid images were similar to human interpretations. From segmentation results, it is possible to establish the ice concentration. Ice concentration from segmentation results was more accurate than AMSR-E which used a passive sensor. The reason is originated from a difference in resolution. High resolution SAR images allow more detailed estimation of the ice concentration. The proposed method is anticipated for being utilized in other sea ice researches. In addition, an estimation method for ice concentration is going to be used for researching the accurate surface albedo. Therefore I think it is possible that the future climate change research will uses more accurate sea ice distribution and other properties with the proposed method.

Keyword : Sea ice segmentation, MRF Segmentation, Local Fractal Dimension, Synthetic Aperture Radar (SAR)

Student Number : 2010-20351

Table of Contents

List of Tables

List of Figures

1. Introduction

The climate change is a public issue and a well-known topic. The climate change has thought that it is accelerated by the carbon emissions from human activities. In this manner, some scientists are called as the anthropogenic climate change [1, 2]. In fact, the climate is a crucial factor of ecosystem. Thus the rapid changing rate of climate could be a problem. Some researchers worried about the extinction event of animals [3]. In addition, the changed climate has brought massive natural disasters. To reduce the effect of climate change, many researchers has endeavored to understand the climate system and tried to predict future climate. The simulation of climate system is an active research area for this purpose. In this simulation, a lot of climate models are using the sea ice property as a key variable [4, 5].

The sea ice is closely connected with the polar climate system. There are several roles of sea ice in polar climate. First of all, the sea ice has high albedo which is a fraction of the reflected solar radiation compare to the total incidence solar radiation. Usually, the sea ice reflects most solar radiation and it drives a cold climate in polar region. On the contrary, the open water has low albedo and heating itself. This mechanism controls the energy budget of the polar region and explains why the polar region keeps cold climate. Another role of the sea ice is an insulator between the ocean and the atmosphere. Thick sea ice effectively prevents a heat exchange from ocean to cold polar atmosphere. For these reasons, the sea ice properties are the important factors to interpret the polar climate. Thus, for more reasonable future climate estimation, many researchers want to get meaningful and reliable sea ice properties especially a distribution and an albedo.

Recently the sea ice extensions dramatically diminished. It allowed a possible polar maritime transportation route.[6] Actually, the sea ice

extension is suffered seasonal variation, so the polar route is not always ready. In addition, harsh weathers in polar region could be an obstacle for the polar route. These obstacles on the polar transportation route are also related to the polar climate especially the sea ice distribution. Consequently the sea ice concentration monitoring is very important in polar route development and its manipulation.

For above reasons, the demand of monitoring of polar sea ice has been raised in this decade. Unfortunately, the Arctic and Antarctic are veiled by harsh weather condition. Further, the polar region is covered by snow and ice in most area. In this case, the remote sensing technique is a suitable tool for monitoring the polar region. Among the remote sensing missions, the Synthetic Aperture Radar (SAR) system is well-known for the sea ice observation. SAR system uses an active sensor which radiates the electromagnetic waves and receives the backscattered signal. Due to the active sensor, SAR system can be operated under all weather conditions unlike optical sensors. In addition, SAR system can produce a fine resolution image from relatively small aperture antenna module by synthesizing technique. For these reasons, many satellite SAR programs have been launched and operated for the Arctic and Antarctic investigation purpose. The SAR programs, such as RADARSAT, ENVISAT, TerraSAR-X and so on, are dramatically growth especially in this decade.

Owing to lots of observation programs, enormous sea ice data are gathered. Extracting meaningful parameters, such as, sea ice shape, area, extent, even albedo and so on, is essential for understanding the sea ice evolution and progression. To extract the target information, there is needed a reliable and robust processing algorithm. One possible technique is the segmentation technique which extracts only sea ice portion on target images. Because the segmented sea ice images are easy to manipulate for calculating sea ice properties. In this case, the segmentation is acting like a pre-process algorithm. Recently, many segmentation algorithms are proposed. Some

researchers were used neural network algorithm [7-10]. The others adopted Support Vector Machine (SVM) algorithm [11-13]. Unfortunately, these methods are required a pre-known such as a training set for initial estimation in segmentation procedure. To avoid this burden, I focused on the unsupervised segmentation methods likewise Markov Random Field (MRF) segmentation method [14-21].

The MRF segmentation is a well-known segmentation method. It is a probability model based segmentation which assumes an image follows a probability model. For more details, it parameterizes two aspect of each pixel. First is the distribution of the magnitude of each pixel. Second aspect is the texture property of each pixel and its neighbors. The MRF segmentation deals with these aspects by utilizing the Gaussian distribution based Maximum Likelihood Estimator[22] and the clique potential energy[23] of each pixel groups. With these two functions, the MRF segmentation makes a new cost function and perform the optimization procedure.

In this study, the Local Fractal Dimension (LFD) [24-27] was utilized to remark sea ice region in the SAR images. If the only sea ice region is represented in certain metric, it would be used for the classification. Really, the LFD value of the sea ice is higher than other region. So the LFD is usefully used to enhance the sea ice detection accuracy. For more details, the LFD utilizes the sea ice texture character in adjacent pixel groups. Actually the typical sea ice surface has a few centimeter scale height which is rough surface in viewpoint of the SAR sensor. In Fig. 1, the arctic sea ice photograph is given. In addition, the sample SAR images of the sea ice and open water are represented in Fig. 2. In the microwave frequency, the SAR system depicts the sea ice area as a heterogeneous bulk region in upper right in Fig. 2. The Fig. 3 shows the actual pixel magnitude of the local sea ice region. This image indicates that a flat sea ice fragments could be presented with different digital numbers.

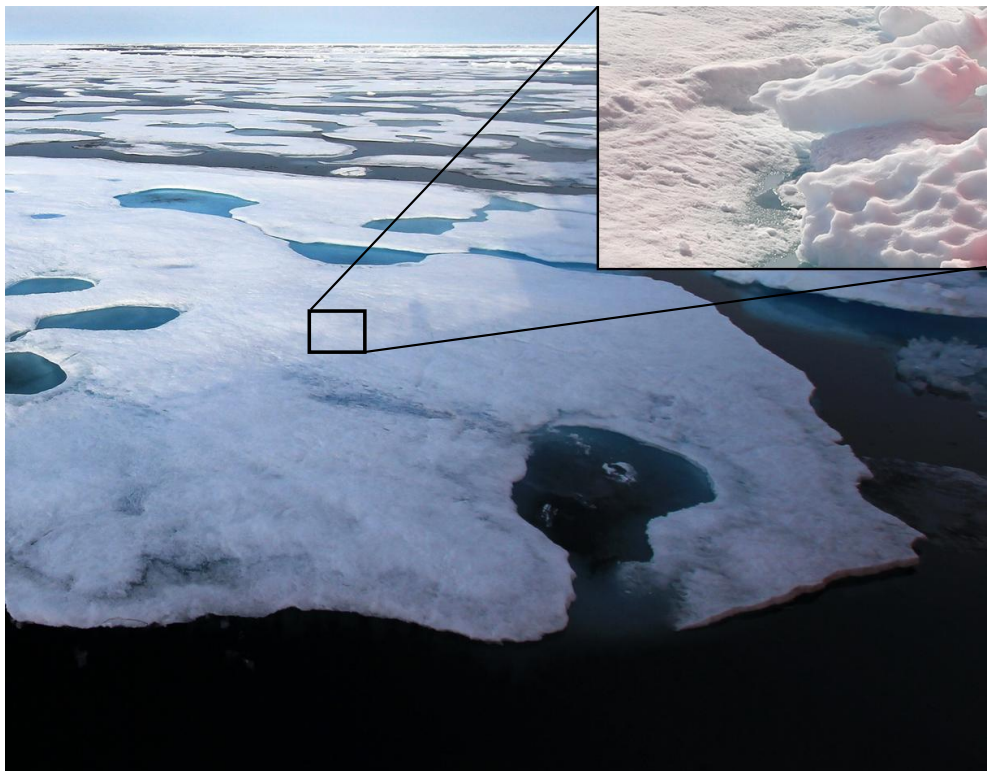

Fig. 1. Photograph of the Sea Ice in the Arctic Sea

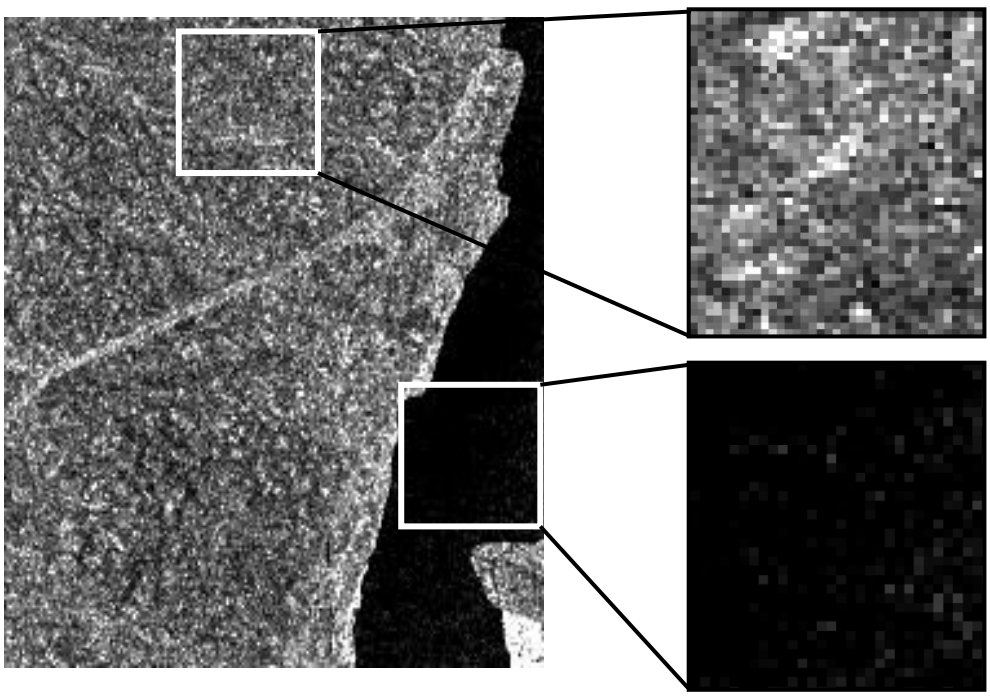

Fig. 2. Magnified SAR image on the Sea Ice and the Open water

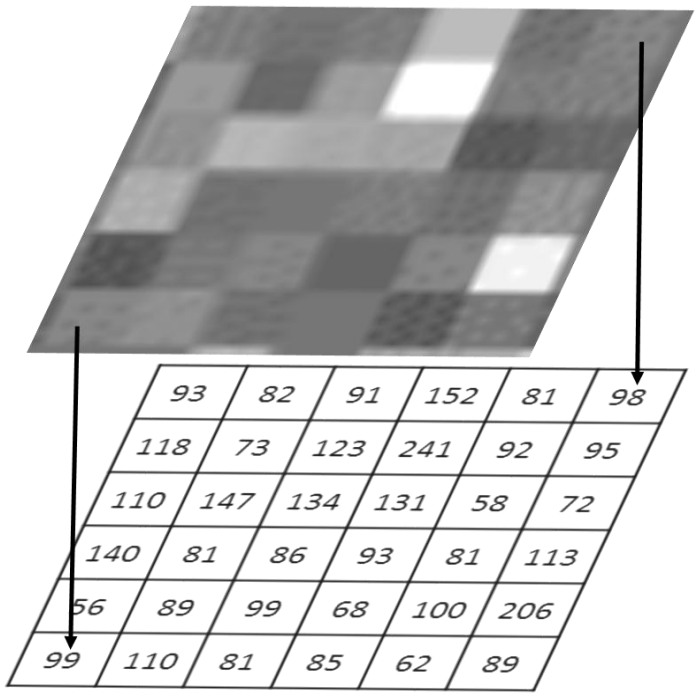

Fig. 3. Pixel Magnitude of Partial SAR image

The LFD is determined a high value on heterogeneous region likewise the sea ice region. It is originated by the definition of the fractal dimension. The fractal dimension was introduced to measure the randomness of the nature in the beginning [28]. The LFD also follow this concept. The LFD is established by magnitude variation and its distance in local pixel group. These information are closely related with the randomness of the region. In this manner, the LFD could remark the heterogeneity in local sea ice region. On the contrary, the open water is looked like a relatively dark and homogeneous region. Consequently, the LFD is a powerful tool for separating the sea ice and open water in SAR image.

2. Background

This study combined the MRF segmentation method and the LFD from the SAR images. MRF segmentation method is assumed that the image is followed certain MRF probability model. With this assumption, the pixels in the image could be dealt with probability parameters. Actually, the stochastic parameters are estimated and updated in every iteration stages during segmentation procedure. The MRF segmentation uses the clique potential to describe the local texture of pixel group. By these schemes, the cost function of the MRF segmentation process is developed. The assimilation methods are investigated by some researchers [16-18]. These approaches could be interpreted as a weight determination of two functions. In this study also adopted some concept of the weighting method. The actual segmentation procedure is similar to the EM (Expectation-Maximization) optimization algorithm. The parameters of each class of the cost function are guessed and updated. After that, the cost function calculates a criterion for determining the most feasible class of the pixel under the probability model.

The LFD is derived by the Quadratic Self-Correlation (QSC) method with normalized integral fit [24]. The QSC method exploits the dynamic range of the local region and its radius. To acquire a robust result, the fractal dimension is calculated by QSC method in several radius cases and performed the graph fitting. This fitting is performed on the normalized log-log plot with the fractal dimension and its radius. It can be converted as an integral calculation because of the normalized graph. By this integral, it can be got the more reliable fractal dimension value.

2.1. MRF segmentation

It is well-known that the segmentation tasks are interpreted as a

maximum posterior problem in the Bayesian framework. It is focus on the dimmed posterior probability from the clear priori probability. It can be expressed as follow equation.

$$x^* = argmax \;\; P(x \mid y) = argmax \;\; P(y \mid x)P(x) \tag{1}$$

The x denotes the class of the pixel and y means the pixel magnitude as brightness. It is a basis of how to classify pixels into a number of certain classes. With equation (1), it is possible to calculate the probability of all possible segmented cases which means the posterior probability. As a result, the segmentation is transformed to an operation which chooses the best probable case among all possible segmented cases.

2.1.1. Feature potential

Many segmentation techniques are utilizes a Gaussian distribution to determine the characteristics of the pixel. In fact, typical images are followed the Gaussian distribution in natural target case. One histogram of sea ice SAR image is presented in Fig. 4. It is made by a SAR image of TerraSAR-X. The SAR image was processed by NEST program as an 8-bit grayscale image. X axis means the magnitude value of pixel and Y axis means the number of pixels which has that magnitude. In this histogram, it is looked that there are two distributions. These two is similar to the Gaussian distribution. Actually, this image is segmented by two classes that sea ice and open water. The histogram of the pixel magnitudes are followed the normal distribution. In this manner, it is natural that using the Gaussian maximum-likelihood concept for estimating the most probable class of each pixel. This idea is the feature potential energy and it is established by above idea as follows:

$$E_{feature} = \sum \left\{ \frac{1}{2} \ln(2\pi\sigma_x^2) + \frac{(y - \mu_x)^2}{2\sigma_x^2} \right\} \tag{2}$$

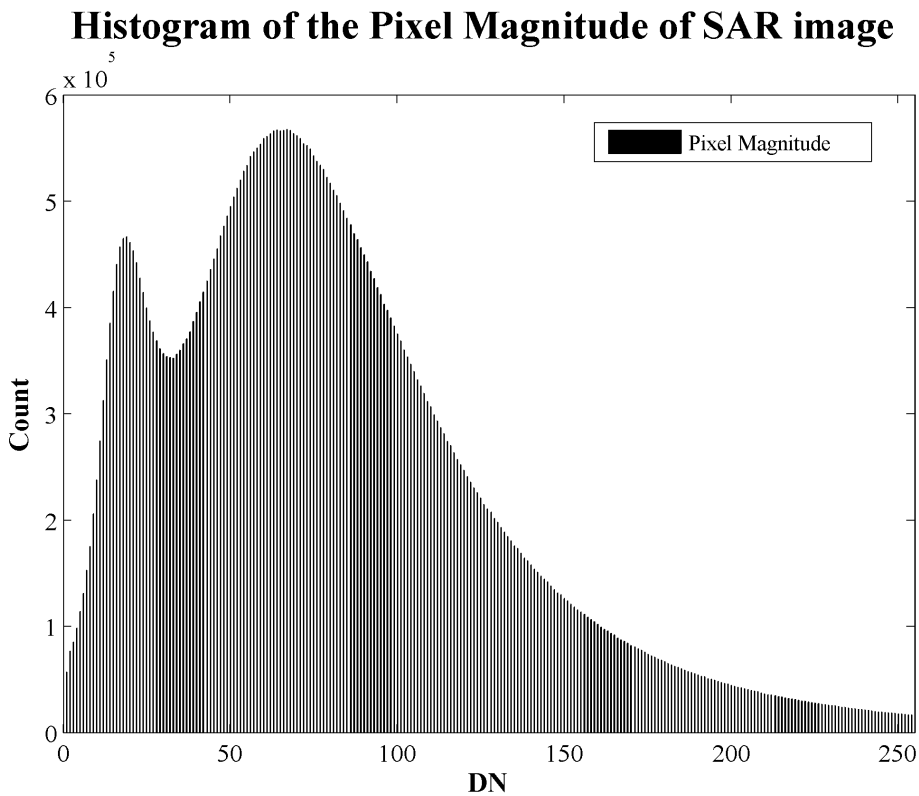

Fig. 4. Histogram of the Pixel Magnitude of SAR image

In equation (2), the x means the class of pixel and the y means pixel magnitude. This equation is similar to the log-like Gaussian maximum likelihood equation. The derivation of equation (2) is given as follows:

In the derivation of the equation (2), the start point is a probability density function of Gaussian distribution.

$$p(y) = \frac{1}{\sigma\sqrt{2\pi}} \exp\left\{-\frac{(y-\mu)^2}{2\sigma^2}\right\} \tag{3}$$

Now, apply logarithm to equation (3).

$$\ln\ p(y) = -\frac{1}{2}\ln(2\pi) - \frac{1}{2}\ln(\sigma^2) - \sum \frac{(y-\mu)^2}{2\sigma^2} \tag{4}$$

For convenience and simplicity, remove the constant term and take away minus sign (-) from equation (4) for making equation (2). It determines the probability from its magnitude. Each class follows different distribution, so the probability of certain pixel is varied by guessed classes. During the segmentation process, probability parameters of each class will be updated in each iteration and the probable class of each pixel will also be determined.

2.1.2. Label potential

The MRF segmentation uses the relationship between interested pixel and its adjacent pixels. This information is parameterized as the label potential in segmentation task. For clique potential calculation, the lattice neighborhood system is introduced. In Fig. 5, the neighboring system and the clique system with 1st and 2nd order are represented. Actual calculation of label energy is derived by the number of clique cases in 2nd order neighboring system.

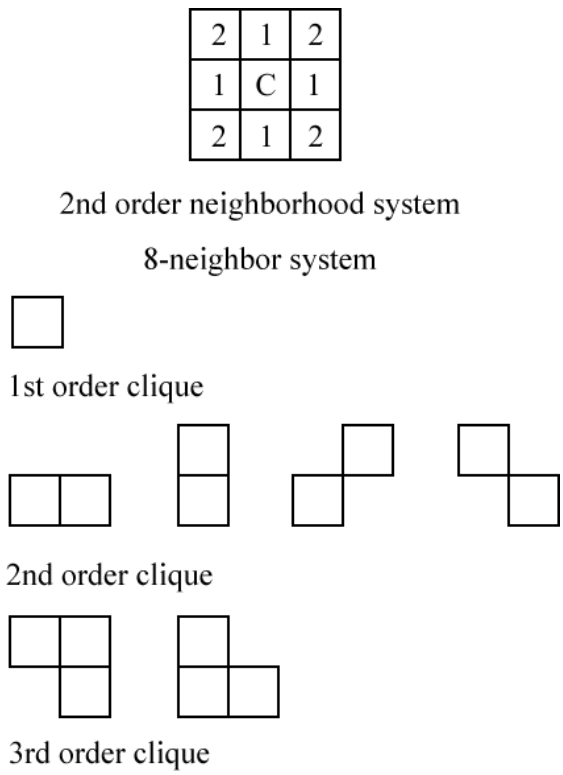

Fig. 5. Neighborhood System and Clique System

The 1st order neighborhood system indicates one middle pixel and connected 4-way pixels. In this case, the possible connections between two adjacent pixels are 3. One is middle pixel itself (connected to oneself). Another combination is horizontal connection and the other connection is vertical connection. Generally, the second order clique system is used to define the label potential. The 2nd order clique system is called 8-neighborhood system. Similar to 1st order system, it is composed to one middle point and 8-way neighbor pixels. The actual calculation of label potential is performed by the kronecker-delta function as follow:

$$U(x_c, x_s) = \begin{matrix} 1 & if\ x_c \neq x_s \\ 0 & otherwise \end{matrix} \quad (5)$$

The x_c and x_s states the class of center pixel and adjacent pixel respectively. The label potential has low energy if a pixel surrounded by same pixels. On the other hand, heterogeneous region has a high label potential. By this approach, it is parameterized the texture information.

The label potential states a sort of similarity in local pixel region. If pixels are same in 2nd order neighboring system, it seems one region and has low label potential. On the contrary, the heterogeneous region has high label potential. In the optimization process view, the cost function should be minimized. By the equation (5), the label potential makes the homogeneous relations to minimize the potential energy. It is same as the clustering of same class of pixels in small region, in the view of the segmentation process. In this manner, the equation (5) is successfully corresponding to the purpose.

2.1.3. Cost function

The MRF segmentation uses a cost function which is a combination of two potential energies as follow:

$$F_{\cos t}\left(\Sigma\left\{\frac{1}{2}\ln(2\pi\sigma_{x_c}^{2})+\frac{(y_c-\mu_{x_c})^2}{2\pi\sigma_{x_c}^{2}}\right\}+U(x_c,x_s)\right) \quad (6)$$

The MRF segmentation eagers to find an argument x_c for minimizing the cost function. It is a finding process that the most probable class from pixel magnitude and adjacent pixel relationship. In this study, it is limited the x_c interval within 0 to 1 for making binary result. Because the binary results are easily presents the sea ice distribution shape.

2.2. Local Fractal Dimension

The LFD is established by the Quadratic Self-Correlation (QSC) scheme in this study [24]. In QSC method, LFD is derived from the Hurst exponents in local region. The Hurst exponents are determined by the dynamic range of each small region and radius of region. The small regions are selected by one pixel and adjacent pixels within certain radius in designed window region. These Hurst exponents determine the LFD of window region by a regression process. Fortunately, this regression can be converted to the normalized integral fit in normalized graph. This normalized graph is consisted by two normalized axes. One is normalized logarithm magnitudes and another is normalized logarithm distances per radii. Detail explanation will be given in section 2.2.2.

The LFD result is located between [0, 1] interval. Actually, the fractal dimension of 2D images should be locate in [2, 3] interval. This difference is simply resolve by adding 2 on LFD result. However, in this study, the LFD is utilized for the segmentation task. The reason is that the difference allows the separation of different classes in the segmentation process.

2.2.1. Blanket method

Before the LFD calculation, it is needed to review the blanket method for estimation of fractal dimension [29]. It is a conventional method and relatively simple method.

Every image can be interpreted as a terrain surface with its magnitude value. This concept is similar to a digital elevation map. So, the magnitude is considered as a height of a pixel. Now, assume a blanket which covers the surface on upper and lower side with thickness ε. The initial values of two blankets are the magnitude of target pixel g (i, j). After that, upper side goes to upward and lower blanket goes to downward. According to this concept, the equations of two blanket surfaces are iteratively determined as follows:

$$u_{\varepsilon}(i,j) = \max\{\, u_{\varepsilon-1}(i,j) + 1, \max_{d(i,j,m,n)\le 1} i_{\varepsilon-1}(m,n)\} \tag{7}$$

$$b_{\varepsilon}(i,j) = \min\{\, b_{\varepsilon-1}(i,j) - 1, \min_{d(i,j,m,n)\le 1} b_{\varepsilon-1}(m,n)\} \tag{8}$$

The u_{ε} and b_{ε} is the upper and lower blanket, respectively. The ε means the thickness of blankets and it also indicates an iteration number. The $d(i,j,m,n)$ means a distance between two pixel locations that (i, j) and (m, n). With above definitions, the volume of the blanket can be calculated by following equation:

$$V_{\varepsilon} = \Sigma_{i,j}\{u_{\varepsilon}(i,j) - b_{\varepsilon}(i,j)\} \tag{9}$$

Then, the surface area is calculated by:

$$A(\varepsilon) = \frac{V(\varepsilon)}{2\varepsilon} = \frac{\Sigma_{i,j}\{u_{\varepsilon}(i,j) - b_{\varepsilon}(i,j)\}}{2\varepsilon} \tag{10}$$

This area satisfies next relations:

$$A(\varepsilon) = \varepsilon^{2-D} \tag{11}$$

The fractal dimension of this area is D and it can be calculated from equation (11). Commonly, blanket method is applied in whole image region to establish the fractal dimension.

Fig. 6. represents a terrain surface and two blankets. The upper and lower blankets are covers magnitude surfaces from both side. The fractal dimension is derived by a difference between two blankets. The value is

2.2.2. Linear self-correlation (LSC)

Similar to above method, the fractal dimension of the local region is defined in this section. The start point of this section is a self-similarity. To measure the self-similarity, researchers are using fractional Brownian motion (fBM) formalism. It is suitable for describing a non-stationary stochastic process in many natural phenomena. It contains a useful parameter called Hurst self-correlation exponent H. In the image processing case, an extension of this parameter is established as equation (12). It is determined by the maximum magnitude range (dynamic range, ΔV) within radius r from center pixel [30]. The correlation exponent is as follow:

$$H_1 = \lim_{r \to 0} \left\{ \frac{\log(\Delta V)}{\log(r)} \right\} \tag{12}$$

H_1 shall be normalized to agree with the definition of The Hurst exponent. Then, the fractal dimension D is established by $D = 3 - H_1$ with normalized H_1.

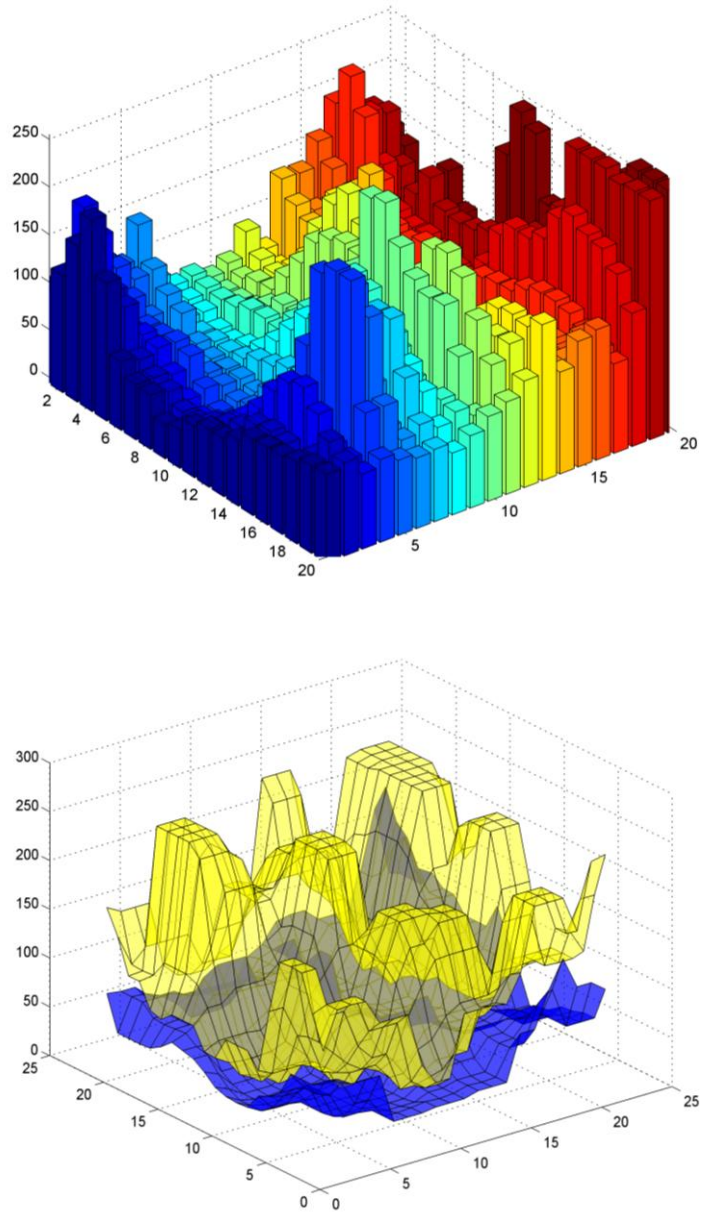

Fig. 6. Blanket Method

By the definition of Hurst exponent, the fractal dimension 2 and 3 means a correlation between pixels. If one pixel has high value, it would affect adjacent pixels. On the contrary, the value 2.5 states a totally uncorrelated relation.

For more reliable result, a regression process was used in this study. The H_1 and related radius were plotted in a log-log graph. With this graph, a closest curve was founded by linear regression. Unfortunately, this approach sometimes produces unreasonable results. For instance, a uniform region made zero ΔV value or 1 radius r region may cause a null value.

2.2.3. Quadratic self-correlation (QSC)

The QSC method is similar to above LSC method. The only different is a change that r^2 rather than r. It is developed to avoid an outlier problem that occurred in LSC scheme. It also uses an extended Hurst exponent concept. An extended Hurst exponent is as follow.

$$H_2 = \lim_{a\to 0}\left\{\frac{\log(\Delta V)}{\log(a)}\right\} = \lim_{r\to 0}\left\{\frac{\log(\Delta V)}{\log(r^2)}\right\} = \frac{1}{2}\lim_{r\to 0}\left\{\frac{\log(\Delta V)}{\log(r)}\right\} = \frac{1}{2}H_1 \tag{13}$$

The $2H_2$ shall be normalized as similar to the H_1 in equation (12). The fractal dimension is established by 3 - $2H_2$ (where, $0 \le 2H_2 \le 1$) has a value between in pixel. In this study, H_2 was calculated by regression rather than the dividing.

One example of the LFD calculation by QSC method is presented in Fig. 7. First, find the dynamic range of this region. It is 185 (=241 – 56). And the width of this region is 6. By the QSC method, the LFD is determined by next calculation:

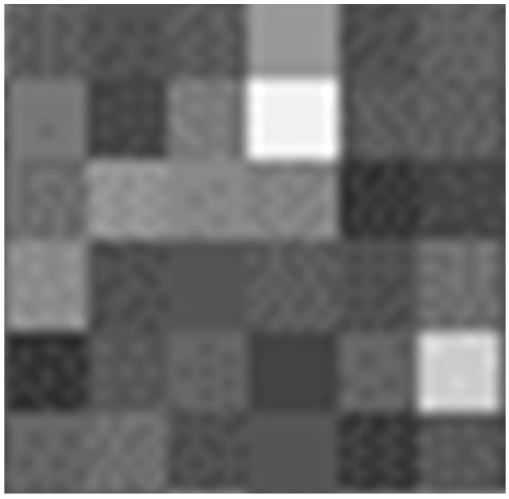

93	82	91	152	81	98
118	73	123	241	92	95
110	147	134	131	58	72
140	81	86	93	81	113
56	89	99	68	100	206
99	110	81	85	62	89

Fig. 7. SAR image and its LFD calculation.

$$(\text{LFD}) = 3 - 2 \times \frac{1}{2}\left(\log(185) \Big/ \log(6) \right) = 2.0579 \qquad (14)$$

The LFD can be determined as equation (14). However, this approach couldn`t satisfy the $r \to 0$ condition. To meet the condition, the regression task is required. Another advantage of the regression is that it allows more reasonable estimation. The LFD results from equation (13) are expressed by logarithm expression. So LFD results are plotted in log-log graph. In this graph, the suitable regression method is least square fitting.

Rather than least square fit, the normalized integral fit is used in this study. Main difference is the axis of the graph. In normalized log radius and normalized H_1 value graph is expressed in Fig. 8. The results of QSC method are located in small circles. The advantage of this plot is that the regression process is converted like an integral task. In other words, the least square fitting line in log-log graph is same as a black horizontal line in Fig. 8. It is originated in the definition of the regression. The linear regression method is a task to find a line which connects the averages in discrete points. These average points are same as the QSC result values in normalized graph. Thus the integral sum which is area under the black sold line is same as the least square fitting task. The final LFD value is determined as a black line value in Fig. 8.

2.2.4. Manhattan distance

To getting more reliable H, the linear regression was conducted in this study. It was calculated from r and H in certain square window (window size W(odd)). The conventional Euclidean distance produces $\sqrt{2}$(W-1) different distance cases in WxW window region. For more efficient regression, the Manhattan distance metric is used to get more distinct radii.

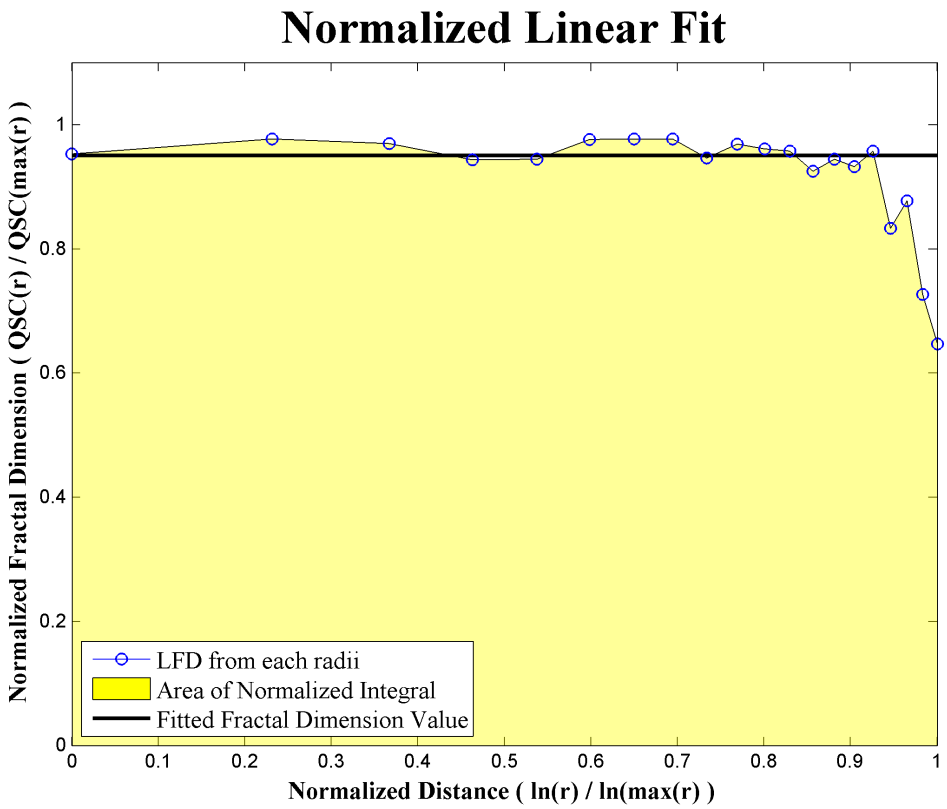

Fig. 8. Normalized Integral Fit

Manhattan distance is known as a taxicab distance. It calculates the distance by counting the movement through a unit length. In other words, it doesn`t allow the diagonal movement. So the final distance is always located on the natural number range. Manhattan distance metric allows the 2(W-1) number of different distance cases in same WxW window. With this metric, the more reliable regression could be possible.

The schematic figure in Fig. 9 shows the difference of the Euclidean distance and Manhattan distance matric. The Euclidean distances are measured by two straight lines which go through the boxes. On the contrary, the Manhattan distances are measured by zigzag lines. The number of difference cases in Euclidean distance is $\sqrt{2}$(W-1). However, the Manhattan distance produces more cases of difference distances as 2 (W-1).

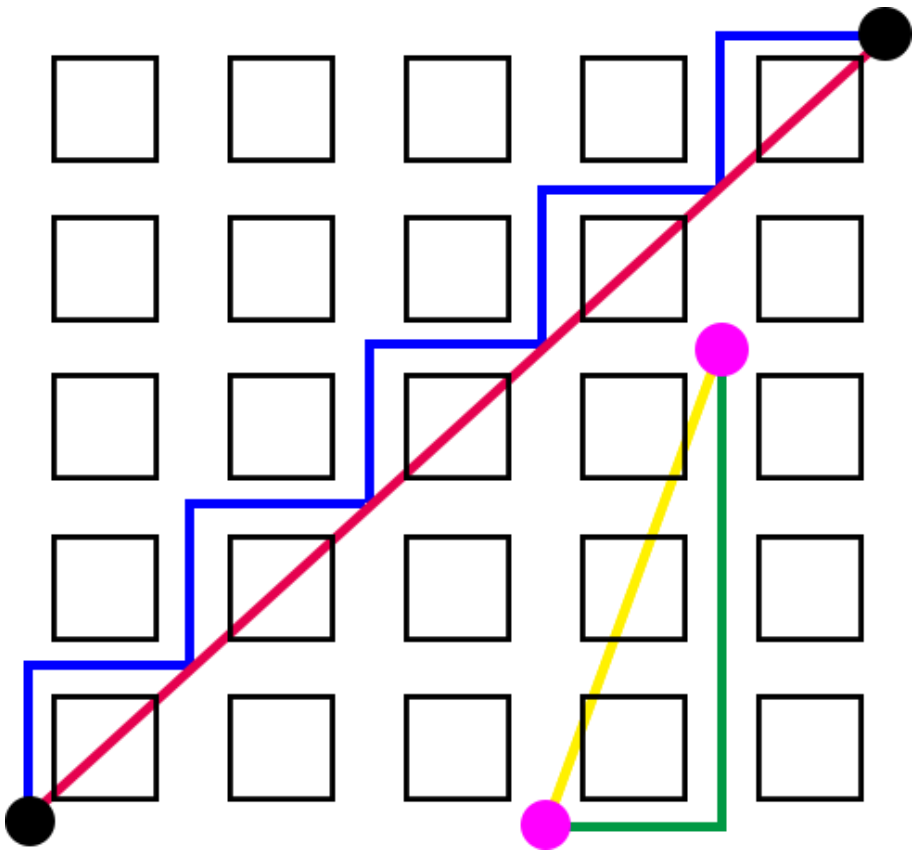

Fig. 9. Manhattan Distance (Taxicab Distance) Metric

3. Data

The used SAR images of this study are listed in Table 1. Two images are taken by TerraSAR-X mission and another is taken by ENVISAT ASAR. TerraSAR-X uses X-band frequency microwave and has 1m spatial resolution. ENVISAT uses C-band frequency. The ENVISAT image is a wide swath ScanSAR mode image.

The ENVISAT image is selected for test purpose. There are several ice types in one image region. This image contains the Thwaites glacier in the Antarctica. Most glacial is located on the land area and some glacial is moved on the sea surface. In the ocean area, there are various types of the sea ice. Major sea ice types are the first-year and multi-year sea ice. The other sea ice types are general stages in melting process of the first year ice. These stages make their own physical properties. It brings a different backscattering coefficient within young sea ice region.

Next, the TerraSAR-X images are taken in summer season. In summer season, the melting process is dominant in sea ice region. Due to this melting, the sea ice in summer season is not clear in the SAR image. Small sea ice is prone to be blurred by Gaussian effect. In addition, an irregular shape of small sea ice fragments brings all kind of scattering mechanisms. It makes hard to recognize an exact location and shape of sea ice. Though, this study tried to find characteristics of a summer season sea ice. Fortunately, the proposed method could separate the sea ice and open water in TerraSAR-X images. The results will be dealt with in result section.

Then, the ice concentration of image region was estimated from segmentation results. The segmentation result represents the location sea ice in image. Thus ice concentration could be established by this sea ice map by simple pixel counting method. This ice concentration results were compared to passive microwave result and in-situ measurements. The AMSR-E data was used in passive microwave category.

Table. 1. Data List of TerraSAR-X images

Date	Location	Polarization
2008. 06. 07.	Beaufort Sea	VV
2010. 08. 10.	Chukchi Sea	VV
2011. 08. 12.	Chukchi Sea	HH

The AMSR-E was served by NASA. It is produced by Special Sensor Microwave/Imager (SSM/I) measurements. The SSM/I contains a seven-channel, passive microwave radiometer sensor. The ice concentration requires the bright temperature data in multiple frequencies. With this data, the ice concentration is estimated in daily basis with 12.5 or 25km spatial resolution.

Beside the passive microwave data, the aerial photographs were used as the in-situ measurement data. They were taken by heli-borne system in the Korean icebreaker, Araon. In helicopter mission, the Gopro Hero action cam was attached and taken sea ice photos. The photographs contain a barrel distortion due to a wide-angle lens. This distortion was eliminated by photoshop lens correction tool.

For clear comparison, actual images are given in chapter 5.

4. Methodology

In this section, the outline of the proposed method will be explained. The proposed method is combination of the MRF segmentation method and the LFD calculation from the original SAR image. Detailed algorithm flow is presented in Fig. 10.

The MRF segmentation could be interpreted as an optimization procedure with a cost function. This cost function in MRF segmentation is consisted by two parts. One is the feature potential and another is label potential. The feature potential calculates a characteristics of a magnitude distribution in local pixel region. Whereas, the label potential determines a relationship between neighboring pixels. Generally the optimization process is performed by EM (expectation-maximization) algorithm approach.

The LFD is used to capture the sea ice texture property in SAR images. In this study, the LFD map is derived by the quadratic self-correlation (QSC) scheme and its normalized integral fitting [5]. To determine the LFD value, a W by W (W: odd) window was defined. Within this window, a dynamic range and its radius were founded and LFD was calculated.

In this paper, the surface of the sea ice was focused especially an irregular shape in a few cm scale (refer Fig 1). It causes the Bragg scattering and brighter than open water area in SAR image. Unfortunately, in X-band sensor view, this sea ice surface is considered as a rough and heterogeneous surface. This feature is originated by microwave scattering mechanism. Backscattered signal magnitude depends on the surface roughness and dielectric constant. Thus sea ice surface make irregular texture on SAR image. For this reason, SAR images express the sea ice region as a textured region. It could be make difference in LFD map between sea ice and open water region. And this information could enhance the sea ice detection in SAR images.

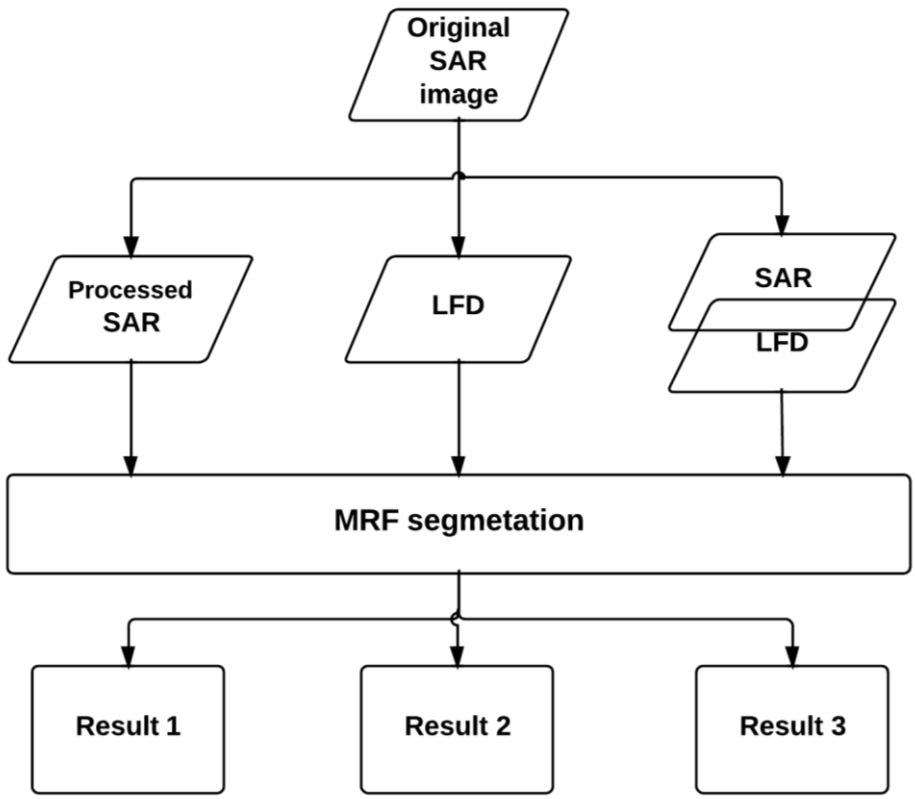

Fig. 10. Flow Chart for Segmentation Procedure

First, I choose several SAR images for segmentation. This SAR image processed with the NEST program which is made by ESA (European Space Agency) under a windows operating system. Output SAR images were constructed as an 8-bit greyscale images. The processing included a speckle noise filter and multilooking with 11x7, 11x6 or 11x9 according to the original image size. In this research, I focused on the SAR images on Arctic region. Selected images were taken by TerraSAR-X mission. Study area is around the Chukchi Sea in summer season. Most of them were contained sea ice floes. For the character of the sea ice in summer season, some ice floes were hided or mixed with other ice types.

With processed images, it is derived the LFD of images by the quadratic self-correlation (QSC) method [5]. It is a possible extent of the Hurst exponent scheme based on the Fractal Brownian Motion (fBM) formalism. The quadratic self-correlation method exploits the dynamic range in local region and radius of region. To acquire a robust fractal dimension, a graph fitting is performed by several radius cases and its dynamic ranges. This fitting feature is comprehended as an integral in normalized fractal dimension and normalized radius. By this integral, it is obtained the more reliable fractal dimension value. One characteristic of LFD metric is the value is located between from 0 to 1 such as a normalized value. In this study, window size of the operation is determined by 5x5. This size was derived by some trial and errors.

Utilized MRF segmentation method is referred from previous MRF segmentation methods [7-9]. MRF segmentation method is assumed that the image is followed MRF probability model. This approach needs probability parameter estimations in each iteration and use the clique potential energy to describe the local texture. The cost function in MRF segmentation method takes into account these two schemes. To assimilate two mechanisms, one simple solution is a method of weighted sum of two portions. By this means, the segmentation is operated as an optimization process with EM

(Expectation-Maximization) algorithm. In each iteration, the parameters from each class are updated and the cost function determines a criterion that the most feasible class under the probability model.

The LFD map is used as an input parameter in MRF segmentation process. To ensure the enhancement, LFD map based segmentation results are compared with other segmentation results. The controlled results are made by original SAR image, normalized standard deviation map in certain window region or its combination.

The class number is fixed as 2 for focusing the sea ice detection quality. By number limitation, some classification results are confused especially SAR image which contains multi type of sea ice regions.

For evaluated segmentation results, I used the unsupervised segmentation criterion [10]. This criterion is developed by the intra-region and inter-region disparity. The criterion has positive correlation with segmentation quality, so higher value is interpreted as a good segmentation result.

5. Results

With described approach, selected SAR image was segmented as the sea ice and the open water region. During this study, the LFD image provided useful information for detecting the sea ice region in SAR images. It is consistent with our assumption.

The results of the conventional MRF segmentation on SAR intensity images did not meet our expectations. The segmentation results were not able to classify the sea ice region only. Whereas the segmentation results with LFD images detected proper sea ice region. It supports that LFD information could provide useful information for sea ice segmentation from SAR images. By this means, the sea ice detection accuracy will be raised.

The results from LFD images had a reinforced segmentation result with clear interface line of the sea ice. In addition, these results shows solid sea ice region without holes. This packed sea ice floes are more similar to human interpretation. In this case, pixels of sea ice region seems more homogeneous compare to the results from SAR intensity images.

The selected ENVISAT image is stated in Fig. 11. With this image, conventional and proposed segmentation methods were conducted. SAR intensity image was used for making Fig. 12. Fig. 13 is shown the segmentation result from LFD image. It was calculated by QSC method with 11x11 pixel window in ENVISAT image. The hybrid image was made by combination of two images (SAR intensity + LFD image). The result from hybrid image is provided in Fig. 14.

As mentioned, this image contains multiple types of sea ice. Some sea ice types are compatible with our assumption. However, other types are different. New ice, was freeze in a few days ago, have a smooth and thin surface. In this case, the radiated waves are reflected from surface. Thus intensity of new ice region is relatively small in SAR image. Open sea also reflects most SAR signals.

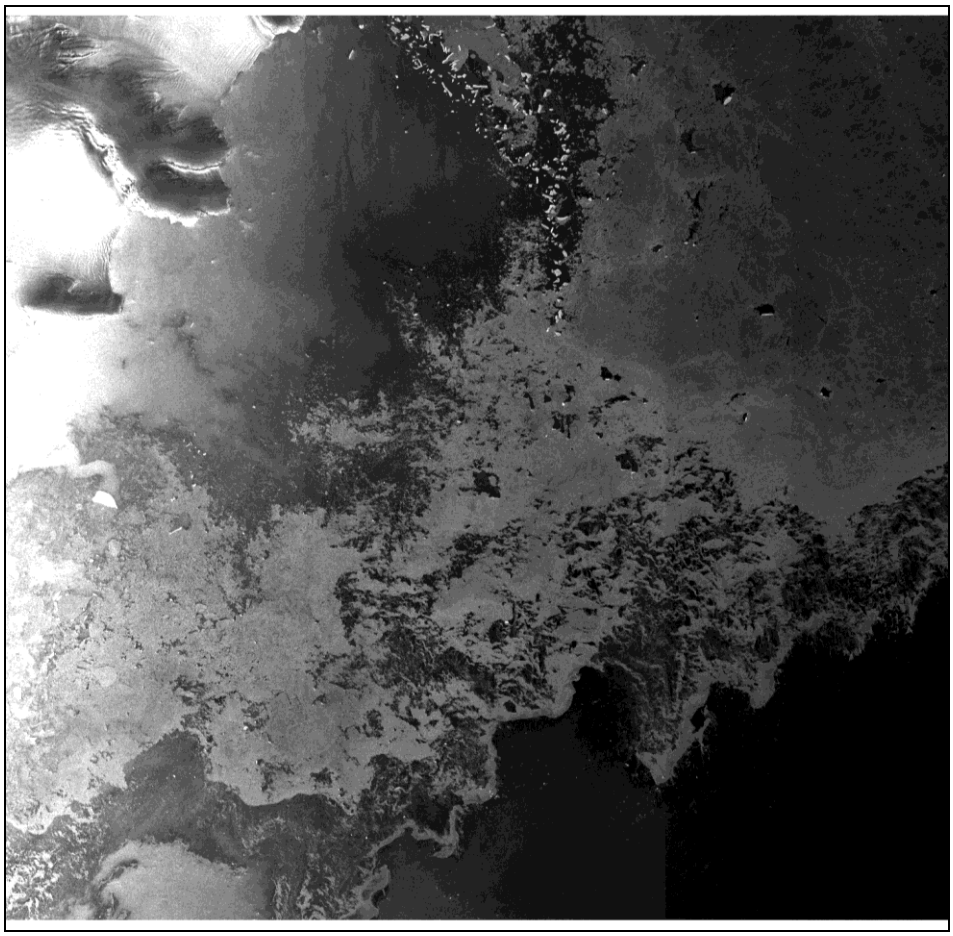

Fig. 11. ENVISAT SAR image

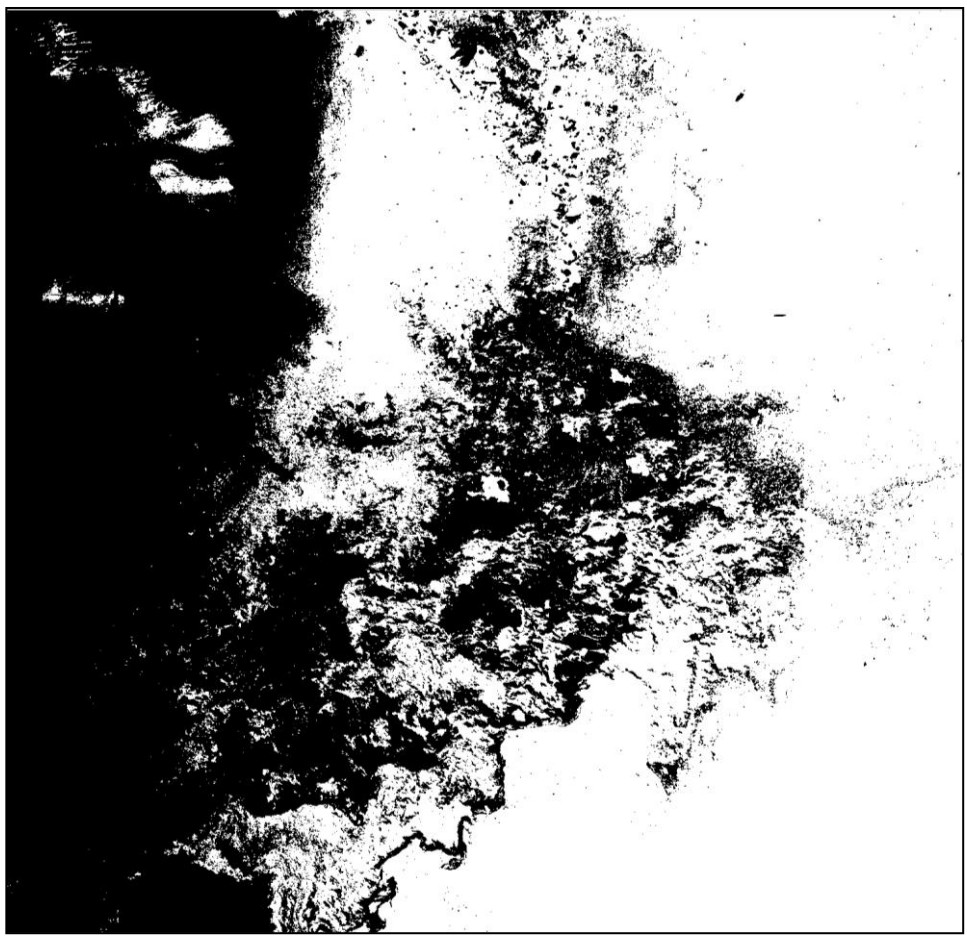

Fig. 12. Segmentation Result from SAR intensity image

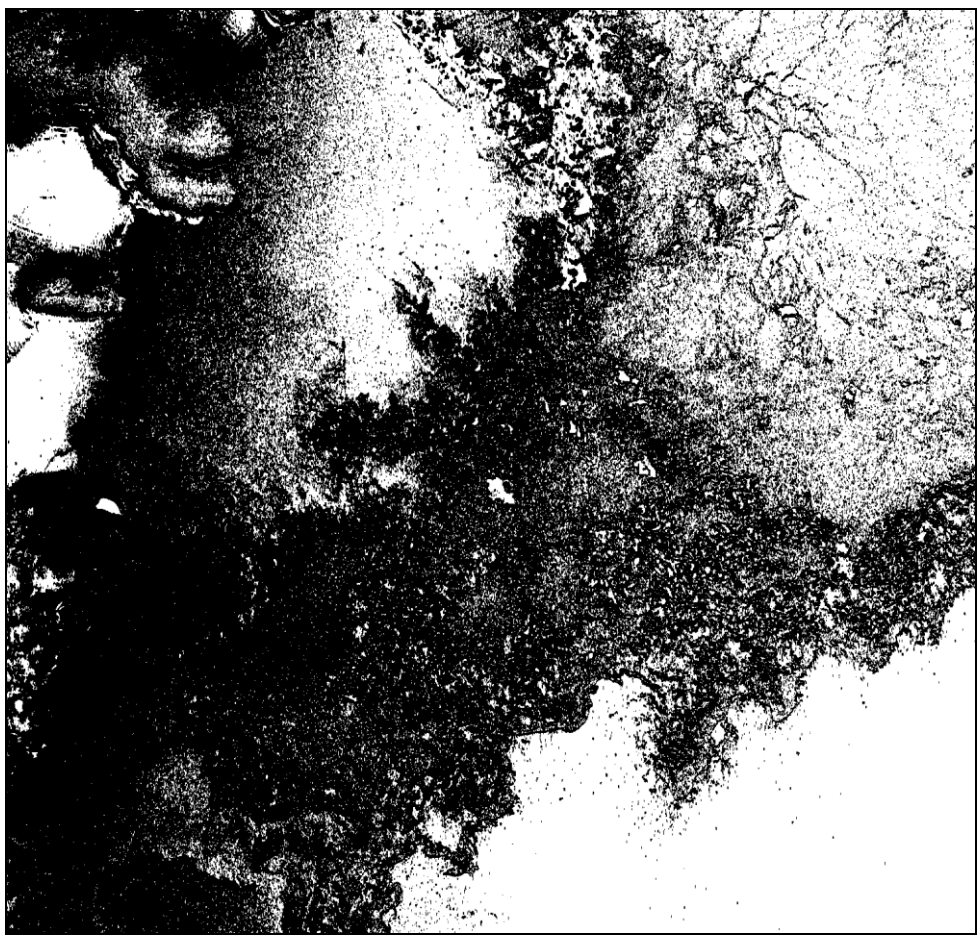

Fig. 13. Segmentation Result from LFD

Fig. 14. Segmentation Result from SAR and LFD

Simple surface scattering mechanism is expressed homogeneous pattern. The homogeneous region has small LFD value. Consequently, the new ice and the open water are apt to be classified same class.

The iceberg is located on the land. Unlike sea ice, it is non saline ice [31]. It means a low dielectric constant and a volume scattering. In this reason, the iceberg region is displayed with higher intensity and homogeneous pattern. It is also different aspect in our assumption.

In this manner, the image selection was not good for testing proposed method. Though, it will provide a guideline for segmentation strategy when applying proposed method.

Look into the segmentation results. The first result (only SAR intensity image input) seems failed to effectively express the sea ice. On the left-side of the Fig. 12, the outlines of the ice floe are not clear. The iceberg region is covered by open water pixels. The interface is fainted and vague. However, the result from LFD, described in Fig. 13, separates the sea ice and iceberg region. Moreover, the sea ice is clearly emphasized in whole image region. Especially, in the multiyear ice region, in upper-right side of image, the ice floes are clearly exhibited with their outline. This prominent advance is not detected in Fig. 12. In fact, it supports our assumption that the LFD is useful information for finding the sea ice in the SAR image.

Secondly, the LFD sometimes confuses in a noise pattern and sea ice fragments. In middle area in Fig. 13, the sea ice shape is not clear unlike Fig. 12. Due to LFD calculation mechanism, there is an ambiguity within the chaotic pattern with homogeneous region in middle of image. To overcome this ambiguity, the hybrid image is used in this study. The result from the hybrid image is represented in Fig. 14. In this figure, the hybrid image produced a clear interface of the sea ice. While the noise pattern is still visible, the sea ice region is clearer and holes are removed.

The segmentation results of ENVISAT image are not perfect. Though, the range of proposed method may be determined from these results.

To focus on the characteristics of LFD, the TERRASAR-X sea ice imageries are selected. First scene was taken on 7th Jun. 2008 near the Beaufort Sea in arctic region. Fig. 15 represents the processed SAR intensity image. It contains both big ice floes and small fragments. There was a melting process in pre-summer season in these ice floes. Big ice floes are easily recognizable and show a typical planar shape. Near the boundary of ice floes, small ice fragments are located. Generally, these fragments are made from a breakup of big ice floes. Especially, the breakup is more frequent in summer due to melting process.

For apply the proposed method, the LFD of TERRASAR-X image was calculated. The LFD image is presented in Fig. 16 with [0.5, 1] interval for strengthening the difference between sea ice region and open water. In this figure, it is clear that the LFD value of sea ice floe is higher than open water. This diversity of LFD is originated in a difference of the scattering mechanism. The open water has a flat surface in microwave frequency. Thus transmitted signals are reflected on the surface and only small portion are backscattered to sensor. On the contrary, the sea ice has a rough and irregular surface. The transmitted signals are mostly backscattered on the sea ice surface and sea ice is represented brightly in SAR image. However, this backscattering mechanism is not uniform on the sea ice floe. An irregular surface shape makes various intensity of backscattered signal. For this reason, the sea ice region has heterogeneous pattern in SAR image and has a high LFD value.

In Fig. 16, the sea ice floes are clearly detectable. The outline of ice floe seems a contour line. It marks the edge of the sea ice region. The LFD image is looked also useful in edge detection method. In the right area, LFD missed the bright fragments. Ice fragments are noticeable in SAR image. The same region in Fig. 16, the LFD values are not even and some area have lower values. The intensity value is even in this area, so the LFD value is low. This situation is not consistent with our assumption.

Fig. 15. TerraSAR-X image (2008. 06. 07.)

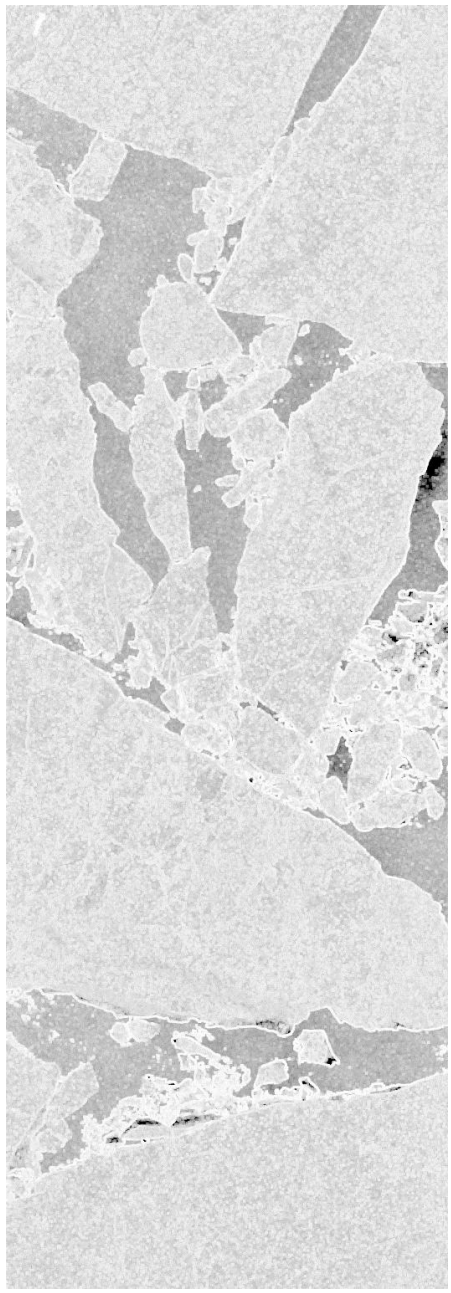

Fig. 16. LFD map from TerraSAR-X image (2008. 06. 07.)

However, this mismatch is not a major difference. Especially in marginal ice zone, the heterogeneous pattern is dominant in sea ice region in SAR image. In this manner, the proposed method could yield a significant advance in segmentation task. Actually the result of this study also supports this assumption.

By proposed segmentation method, the SAR image was segmented. These results are given in Fig. 17~19. The segmentation result from SAR intensity image is Fig. 17. Fig 18 is the result from LFD calculation and Fig. 19 shows the result from hybrid image. In this segmentation, the LFD image is more useful than ENVISAT results. The reason of enhancement is considered that the TERRASAR-X image contains simple sea ice type and the open water region.

The results state that the LFD result provided suitable information for sea ice segmentation. In fact, the result in Fig. 18 is expressed a clear and solid ice floes. While SAR intensity based segmentation provided a dull ice floe shape which contains many holes. It is considered that the distribution of SAR intensity image is not explained by MRF statistics model. So the results are easily biased in an operation.

In addition, LFD result is effective on the relatively dark ice floe region. In right middle side of the image, there are some fragments of sea ice with bright magnitude. It is originated by surface roughness and connected with formation process. Fragments are developed by interaction of adjacent ice planes. This formation is similar to ridge formation within tectonic plate. Due to bright portion is sufficiently bright, this region carries somewhat small magnitude variation within around pixels. In short, the fragments are readily homogeneous and have small LFD value. Though the edges of fragments are detectable, some portion of the fragments is misclassified. Consequently, it is clear that the LFD metric is a powerful tool particularly in multiyear ice detection or ice floe separation procedure. To ensure this, it is performed another segmentation with another SAR image.

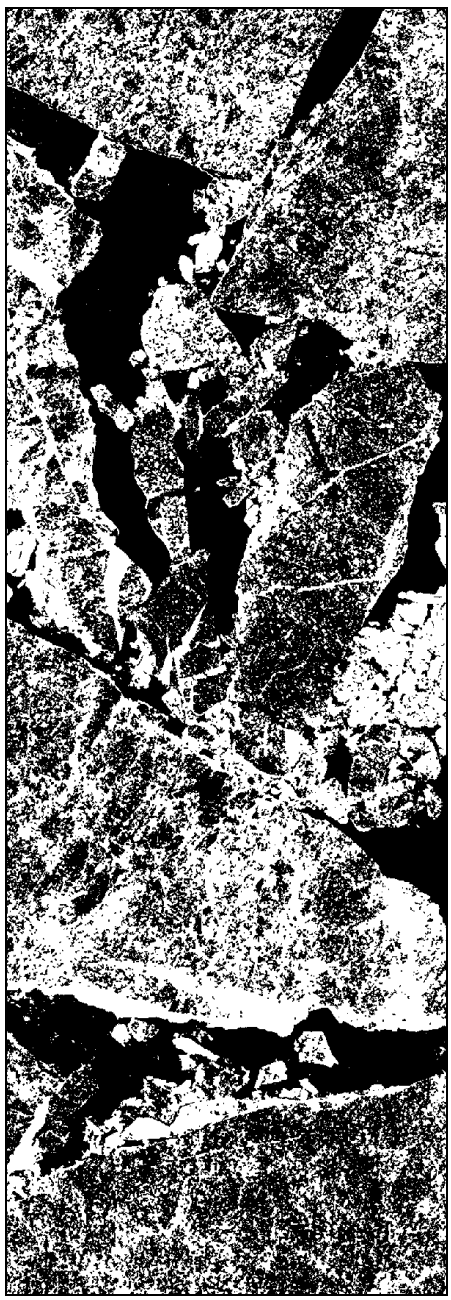

Fig. 17. Segmentation Result from SAR intensity image

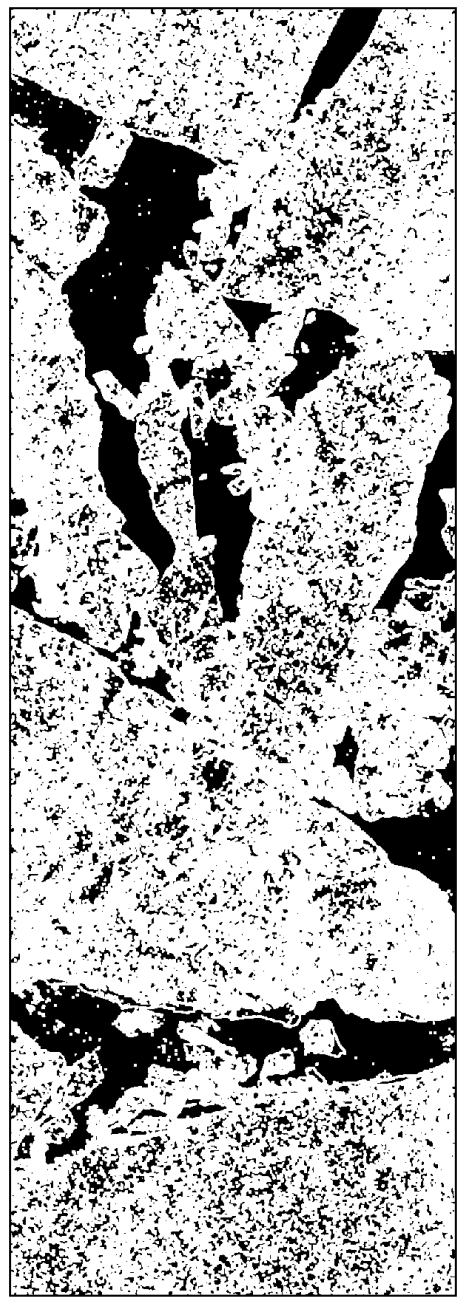

Fig. 18. Segmentation Results from LFD

Fig. 19. Segmentation Result from SAR and LFD

Another TERRASAR-X image is represented in Fig. 20. This image was also taken on the summer season. It shows marginal ice zone with ice floes. Actually, the sea ice covers whole region, however it is not seems like that case. Some regions are not similar to the sea ice pattern.

The sea ice floes are the relatively dark grey spots. The brighter region is covered by first year or young ice. It is believed that there are many cracks and small ridges. And it contains high salinity which is captured from ocean water. The rough surface and high saline make a high intensity value in SAR image. Lastly, the dark region is considered as open water. This portion was covered by new ice as ENVISAT image when SAR image was taken. Consequently, different sea ice types are exhibited as an intensity difference in SAR image. And the mixing of various type of sea ice makes the segmentation worse.

The MRF segmentation result from SAR intensity image is located in Fig. 21. It seems be failed to detect the sea ice floes. The result is looked a chaotic pattern. Sea ice distribution is similar to a cloud in Fig. 21. It is not agree with human interpretation. Further it seems more complex than SAR intensity image.

Conversely, the result from LFD, in Fig. 22, provides the ice floes with clear outline from complicate region. In this case, the LFD helps a detection of sea ice floes. The ice floes are depicted as small particles. It gives help to recognize individual ice floes. In upper side, hided ice floes are revealed which is not separated in the result from SAR intensity image. This result is consistent with an assumption of this study that the proposed method brings an advantage during the sea ice segmentation process.

Fig. 23 represents the segmentation result from a hybrid image. This result display the individual ice floes as same as Fig. 22. However, the shape of ice floes is more simple and clear than the result from LFD. From this result, it is confirmed that the SAR intensity image has a complementary relation with LFD image.

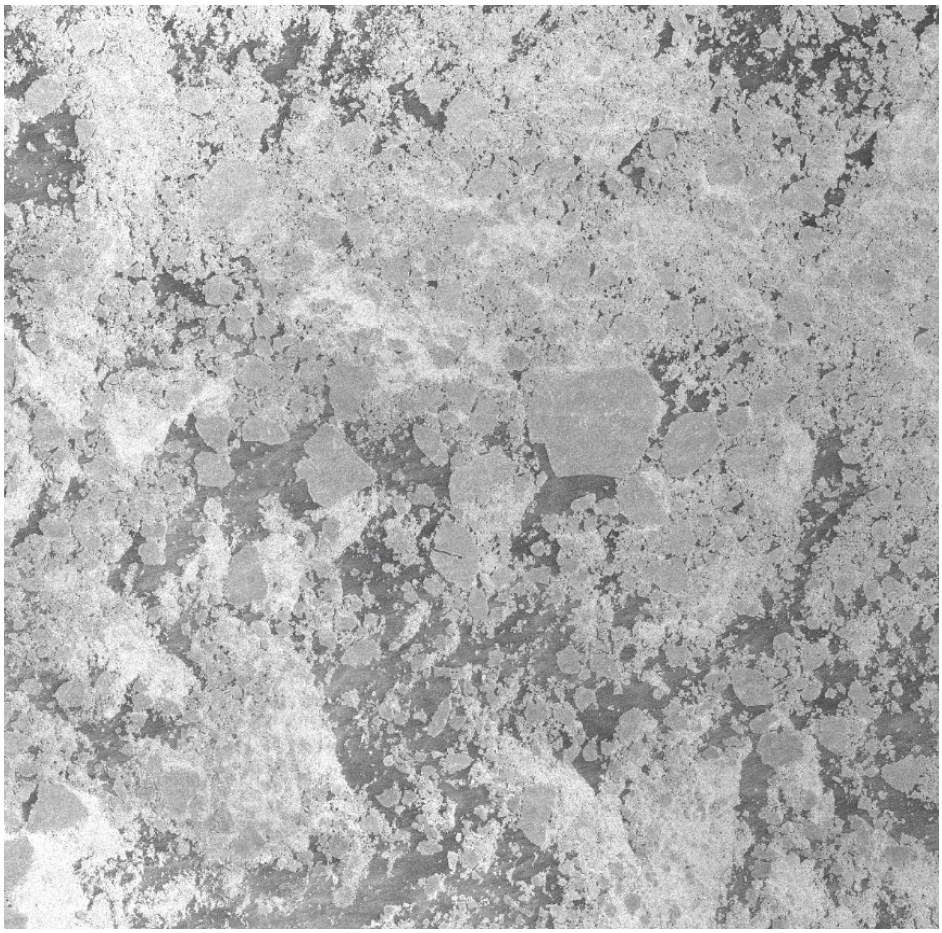

Fig. 20. TerraSAR-X image (2010. 08. 10)

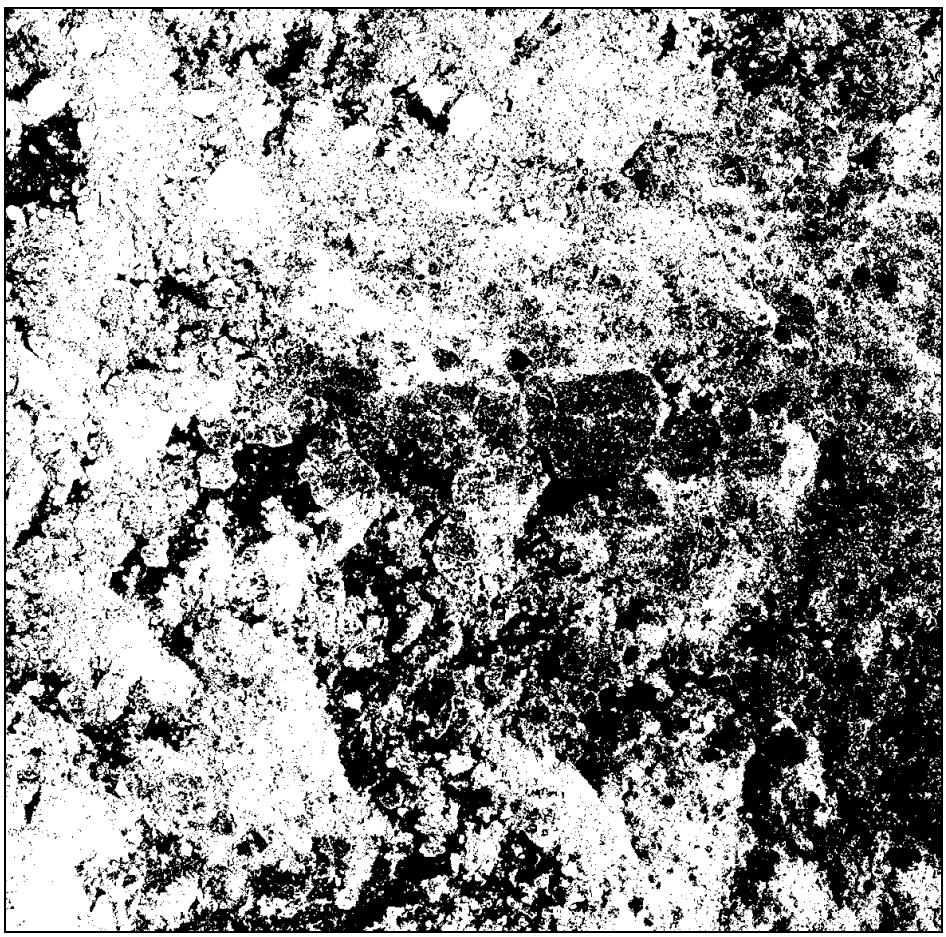

Fig. 21. Segmentation Result from SAR intensity image

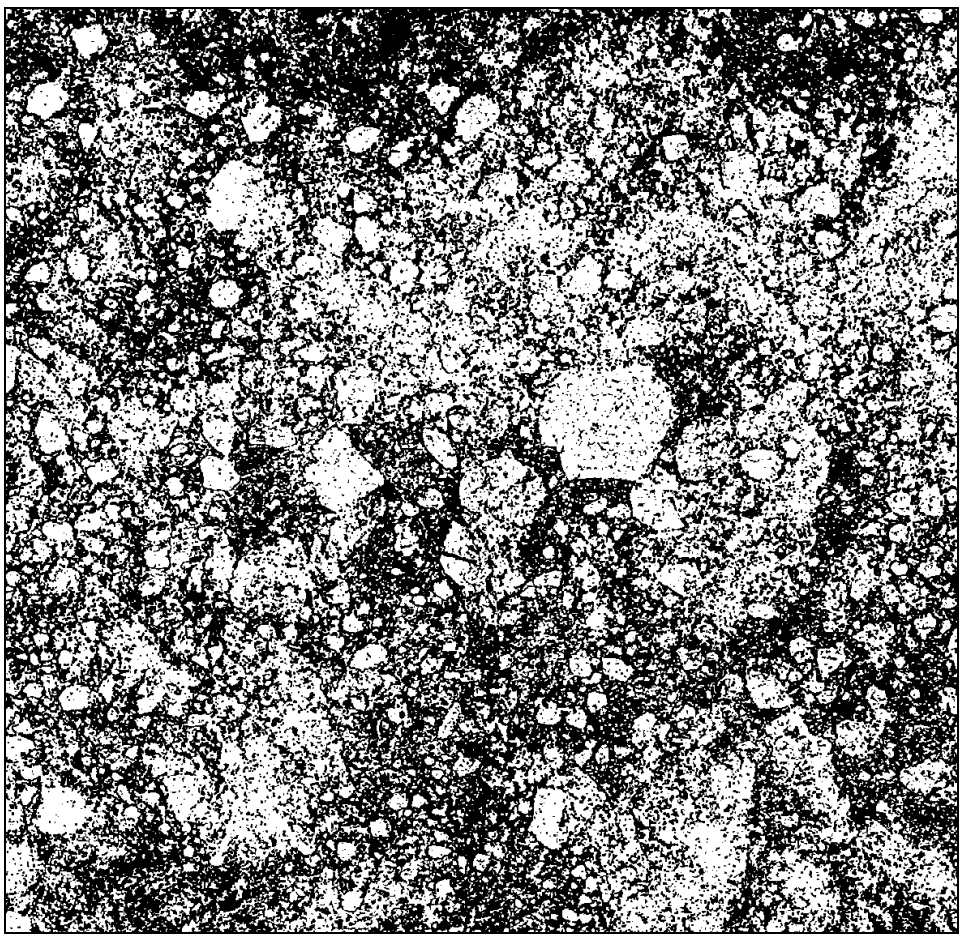

Fig. 22. Segmentation Result from LFD

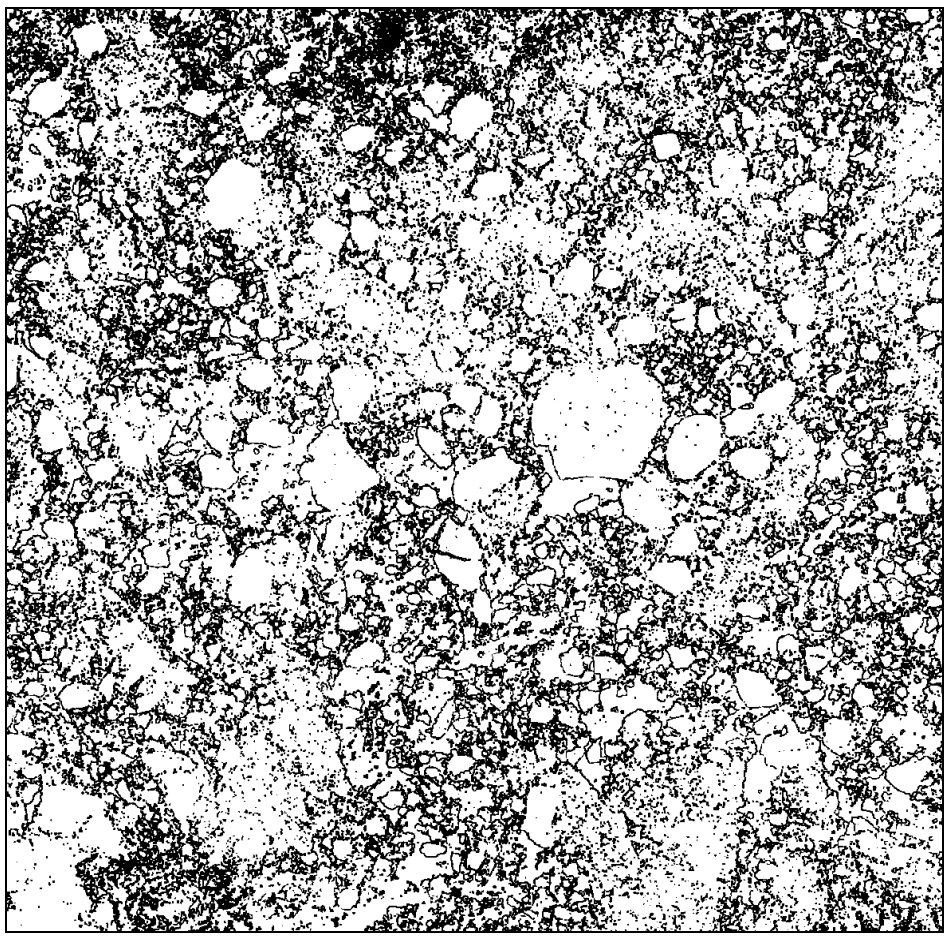

Fig. 23. Segmentation Result from SAR and LFD

Without above TERRASAR-X images, another TERRASAR-X image was analyzed. It is dealt with in chapter 6. The reason is that the segmentation results were utilized for estimating a sea ice property. The estimating procedures and segmentation results will be discussed in discussion section.

For evaluation purpose, an unsupervised segmentation evaluation method [32] is selected in this study. Several unsupervised evaluation methods were introduced and reviewed [33-35]. Among these, simple and reliable method was chosen for this study. The result of unsupervised evaluation method is given in Table 2.

This unsupervised method uses the disparity between the difference classes and the uniformity of each classes [32, 34]. The disparity and uniformity values can be calculated from pixel magnitude values of each class. The disparity measures how difference between the different classes. By the definition of segmentation, the better segmentation should bring larger disparity value. In addition, the uniformity is also inferred by the definition. Intuitively, similar pixels should be classified same class. In this manner, the uniformity condition and the disparity within inter-classes are reasonable terms in evaluation method.

Selected evaluation method is known that the results are correlated with human segmentation [32, 35]. The evaluation results demonstrate the LFD information brings a significant advance in segmentation. In fact, the criteria of the result from LFD and hybrid are higher that the result from SAR intensity image. Roughly the criterion is 10% higher when using the LFD image in segmentation process.

Unfortunately, the criterion value is not an absolute value of segmentation accuracy. Thus another evaluation method is needed for guarantee the evaluation. For this purpose, the reference sea ice map was made by manual segmentation. The manual segmentation follows next steps. First, initial selection was conducted by threshold of pixel magnitude.

Table. 2. Segmentation Evaluation Result

Date	Criteria		
	SAR	LFD	SAR+LFD
2012. 02. 24 (ENVISAT).	0.5724	0.6889	0.6745
2008. 06. 07.	0.6233	0.6938	0.6639
2010. 08. 10.	0.6410	0.6924	0.7221
2010. 08. 12.	0.6727	0.6729	0.6058

Second, sea ice pixels were manually marked by Adobe Photoshop CS6 program. The one reference image and evaluation results are given in Fig. 24 and Table. 3. It was made from 2008. Jun. 7th TERRASAR-X image. In early summer season, the ice floes are not suffered melting process. Thus the ice floes are similar to a big ice sheet. In this manner, the reference image resembles a solid sea ice picture.

The confusion matrix provides a segmentation accuracy of each segmentation methods. The result from SAR intensity image has 76% of accuracy. This result missed much sea ice pixels. But the result from LFD has 86% accuracy. The LFD really detects the property of sea ice region. So the accuracy was dramatically increased. Furthermore, the result from hybrid image has higher segmentation accuracy. Manual evaluation method more obviously shows that the LFD calculation acts an important role in sea ice segmentation procedure.

The reason of the enhancement in the segmentation accuracy is explained by next aspects. First, the LFD captures the sea ice by its heterogeneity in SAR image. This detection helps the sea ice segmentation. Second, the heterogeneity of sea ice is perceived in marginal ice zone. There are ice floes and melting ponds in summer season. In this case, the sea ice has a rough surface by its evolution process. And the scattering mechanism of SAR sensor could bring this characteristic to record SAR image. Third, the proposed method successfully separates the ambiguous pixels especially in sea ice region. Due to this, the sea ice detection rate was increased when LFD image had been used. In addition the disparity also increased in unsupervised evaluation method. Finally, increased detection rate on sea ice pixels makes more solid sea ice classes. By this action, the uniformity calculation indicates the sea ice pixels more uniform and similar in the result from LFD and hybrid cases. Consequently, these results are interpreted the proposed method produce more reasonable segmentation results and similar to human interpretation results.

Fig. 24. Reference Segmentation Image (2008. 06. 07.)

Table. 3. Confusion Matrix (2008. 06. 07.)

		Reference Class	
		Sea ice	Open water
SAR intensity	Sea ice	53.65	0.06
	Open water	46.35	99.94
	Accuracy		76.79
LFD	Sea ice	83.83	10.58
	Open water	16.17	89.42
	Accuracy		86.63
Hybrid (SAR+LFD)	Sea ice	91.37	10.28
	Open water	8.63	89.72
	Accuracy		90.55

(unit: %)

6. Discussion

From now on, this study talked about the LFD image input with Bayesian model based MRF segmentation. With sea ice segmentation results, it is clear that the LFD captures the sea ice properties in SAR image. By LFD calculation, the proposed method produced more reasonable segmentation results. Particularly, the segmentation results on summer season sea ice contain clear ice floes. This result is consistent with human interpretation.

Generally, the sea ice in summer season has an irregular and chaotic shape. And this sea ice is composed of small ice floes and fragments. Moreover, the small sea ice fragments are easily blurred due to the sensor resolution. Though this difficulty, a research on the melting process of sea ice is greatly needed to understand the sea ice evolution. And it is also required to estimate the sea ice characteristics. Eventually, this estimation will be connected to the global climate modelling and future climate expectation. To achieve this goal, the proposed method is considered a suitable tool for this research.

From reasonable segmentation results, the sea ice concentration is estimated in this study. This estimation is determined by finding a pixel fraction in entire image. In this calculation, the sea ice segmentation results are appropriate data.

To establish the ice concentration, a TERRASAR-X image on 2011. Aug. 12^{th} was selected in this study. Fig. 25 represents the selected SAR image. One reason of selection is data acquisition and accessibility. The in-situ measurement and TERRASAR-X shot occurred same time in August 12^{th}. And the AMSR-E ice concentration data on same day was possible to access. It is taken from passive microwave sensor. It has similar scattering mechanism, but it has low resolution. Therefore, the validation of estimation of ice concentration was conducted with two different types of data.

Fig. 25. TerraSAR-X image (2011. 08. 12.)

Conventionally, the ice concentration data has been estimated by passive microwave sensors. The AMSR-E mission is well-known for this estimation. This mission measured the ice concentration of two polar region per daily basis. AMSR-E ice concentration is established from a surface temperature in certain frequency (19, 89GHz) and sea ice type information [36, 37]. One disadvantage of using passive microwave sensor is a poor resolution. AMSR-E data has 25km or 12.5km resolution. It is good for entire earth coverage, but it could not provide subtle information in certain region. For this reason, AMSR-E and fine resolution SAR image comparison researches are conducted [38, 39]. This comparison results stated that there was a different between passive and active microwave sensor remote sensing due to the resolution difference and data coverage problems.

In Fig. 26, the AMSR-E data on 2011 August 12th is provided. It was taken the entire Arctic sea. In this study, the TERRASAR-X image coverage is cropped in AMSR-E data. This is for a comparison purpose and the location is above the Chukchi Sea. Due to the resolution scale difference, SAR image is covered by a few pixels in AMSE-E data.

In addition, an aerial photograph in Fig. 27 shows the actual site condition. The sea ice was melted, so the surface is not fully covered by sea ice. It is the typical aspect of the late summer season sea ice [40]. The melting ponds are wider and wider to cleave the ice floes. From the aerial photograph, the actual ice concentration of SAR image reason could be established. With this result, the ice concentration from sea ice segmentation result could be validated.

The reference ice concentration was produced from aerial photograph. The MRF segmentation was conducted on the aerial photo and finds one ice concentration value. The image coverage scale is also a problem between the aerial photo and SAR images. For comparison, several photos were selected and compared to similar region in SAR image.

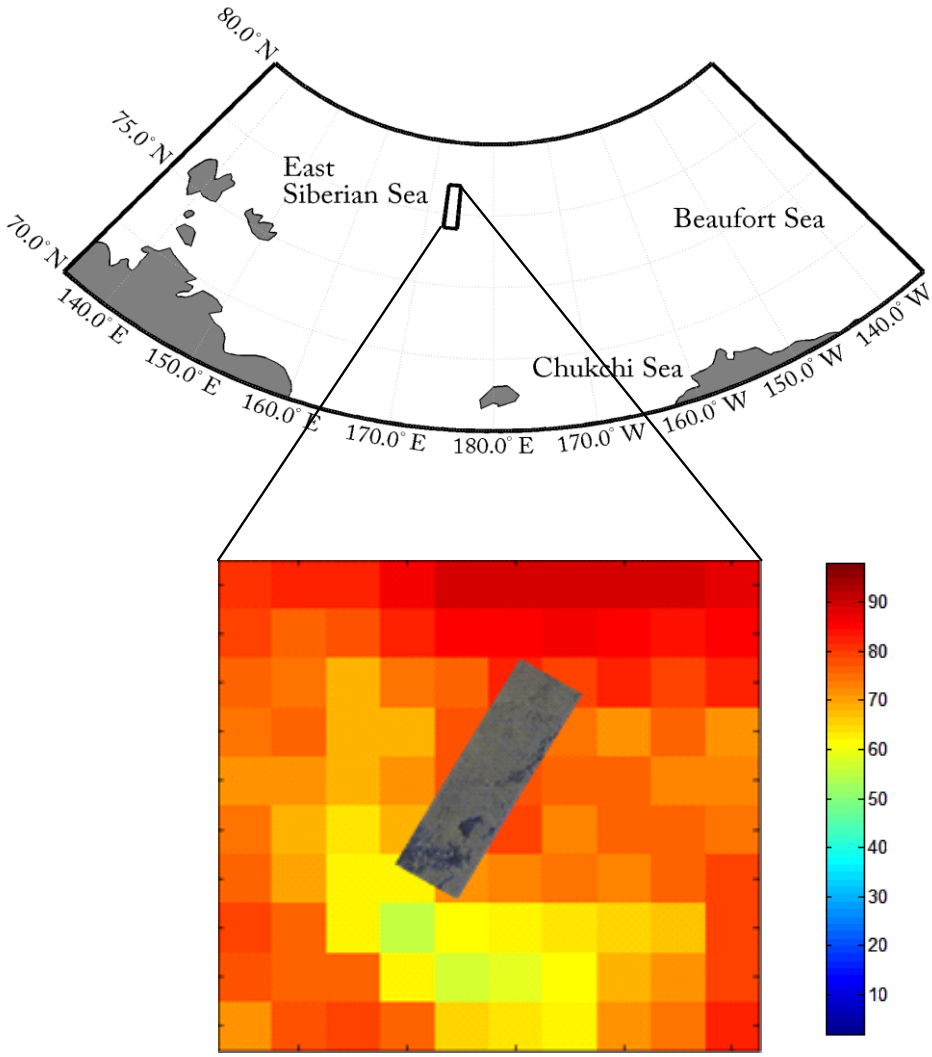

Fig. 26. Ice Concentration data from AMSR-E on 2011. 08. 12

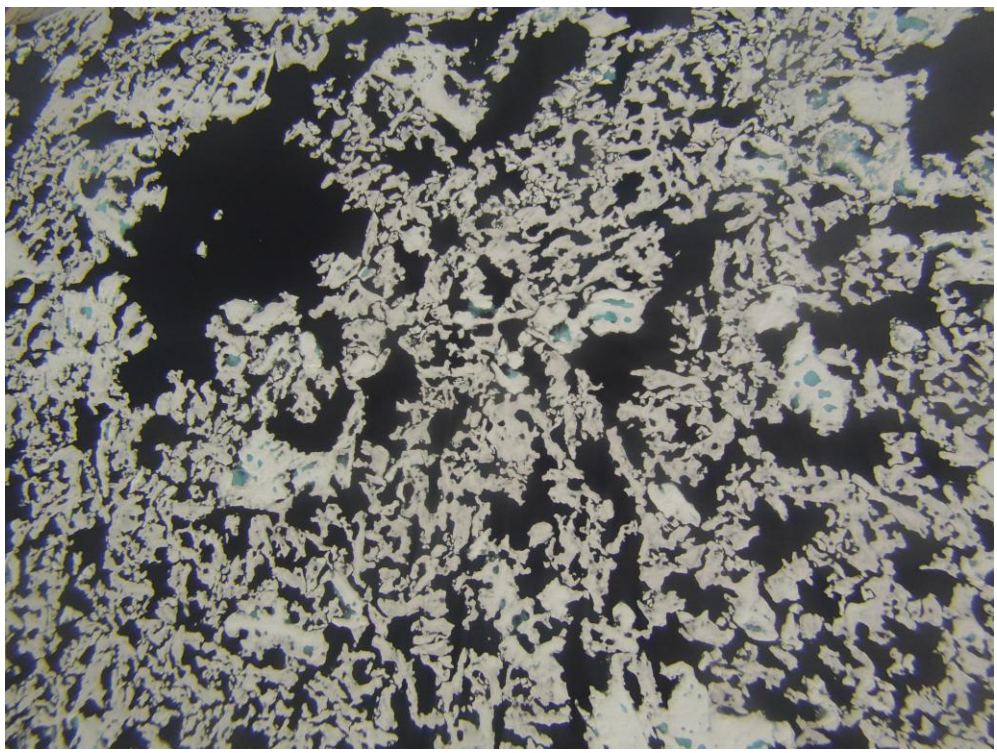

Fig. 27. Summer Season Sea Ice Photograph

With TERRASAR-X image on August 12th, the same segmentation procedure was processed. The segmentation results are presented in Fig. 28~30. The result from SAR intensity is an underestimated result. Most regions are classified as an open water pixels. It is failed to find sea ice region. The result from LFD is an advanced result as anticipated. And the hybrid image created a suitable segmentation result. The result from 2011 August 12th still assists the assumption of this study. The proposed method established more accurate sea ice concentration results. This method helps an estimation of a sea ice property.

The open water region is strengthened in Fig. 28. One possible reason is intensity of sea ice region. The sea ice pixels had relatively small intensity due to contained melting ponds. In fact, a surface of melting pond was relatively smooth, so it reflects most radiated microwave. This mechanism generated an intensity reduction in sea ice region. Reduced intensity caused indistinguishable situation especially in edge of ice floes. Thus some sea ice pixels were misclassified as open water pixels.

In Fig. 29, there are some dark spots in ice floes. It is considered a flat region which has a similar tendency. This defect easily removed by using SAR intensity information. Actually, the Fig. 30 prohibits these spots. Such as previous segmentations, the result from hybrid image shows the best segmentation result. It is looked reasonable sea ice distribution.

With these segmentation results, the ice concentration was determined by pixel counting. The calculated ice concentration values are represented in Table. 4 in Multilook column. This result is agreed with Fig. 28~30. Though, the aerial photo states this region is not fully covered by sea ice. In this view, this first attempt was looked an overestimated result.

To overcome this limitation, original SAR data was re-processed without multilooking. This singlelook image is given in Fig. 31 upperleft image. It is a partial image of Fig. 25 due to calculation cost. And calculated results from singlelook image are located in Table. 4 in Singlelook column.

Fig. 28. Segmentation Result from SAR intensity image

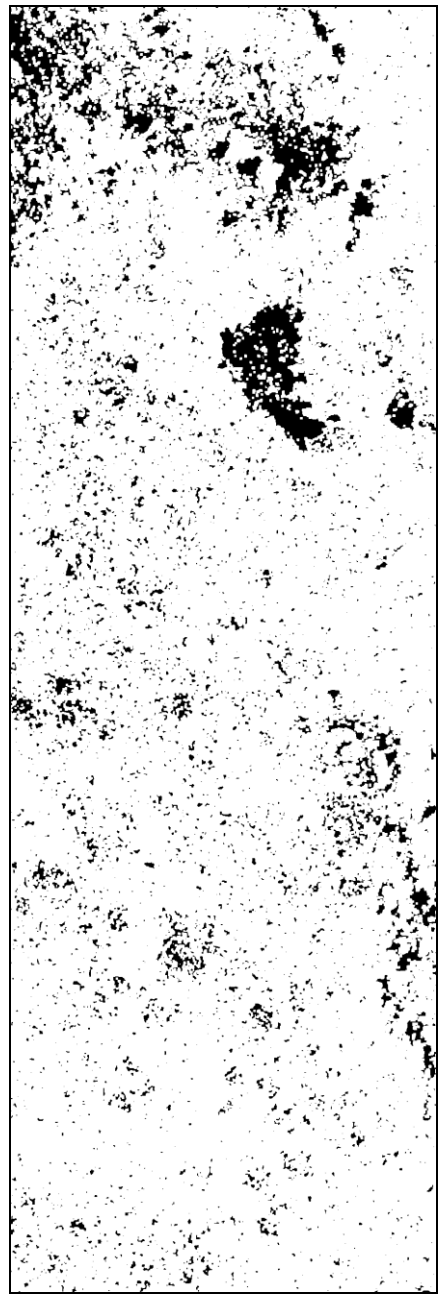

Fig. 29. Segmentation Result from LFD

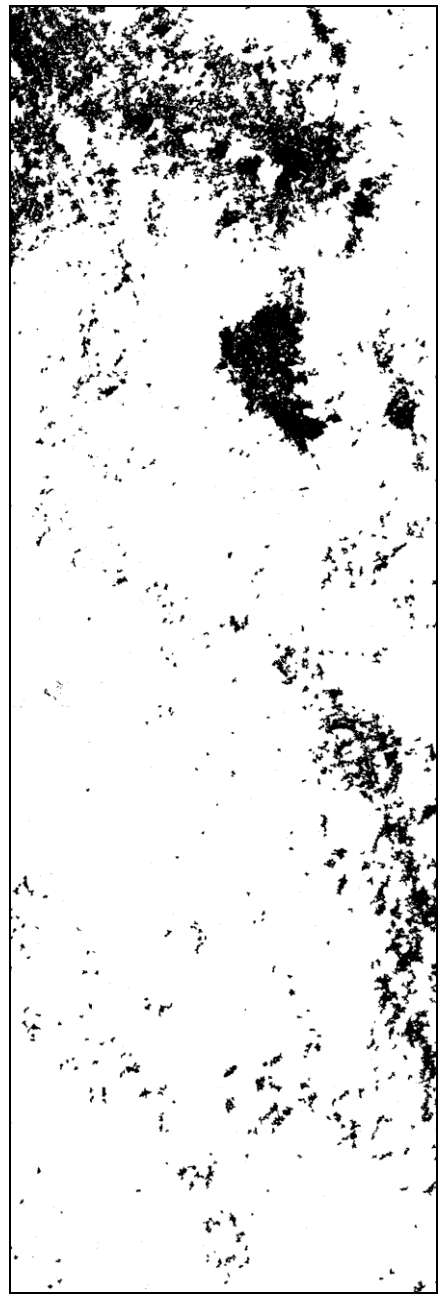

Fig. 30. Segmentation Result from SAR and LFD

Table. 4. Ice Concentration Results from SAR image

Ice Concentration (%)		
	Multilook	**Singlelook**
SAR	40.9324	42.4949
LFD	91.3809	60.4465
SAR+LFD	91.9753	59.4169

※ The AMSR-E ice concentration is located between 73.55%. (Refer Fig. 26)

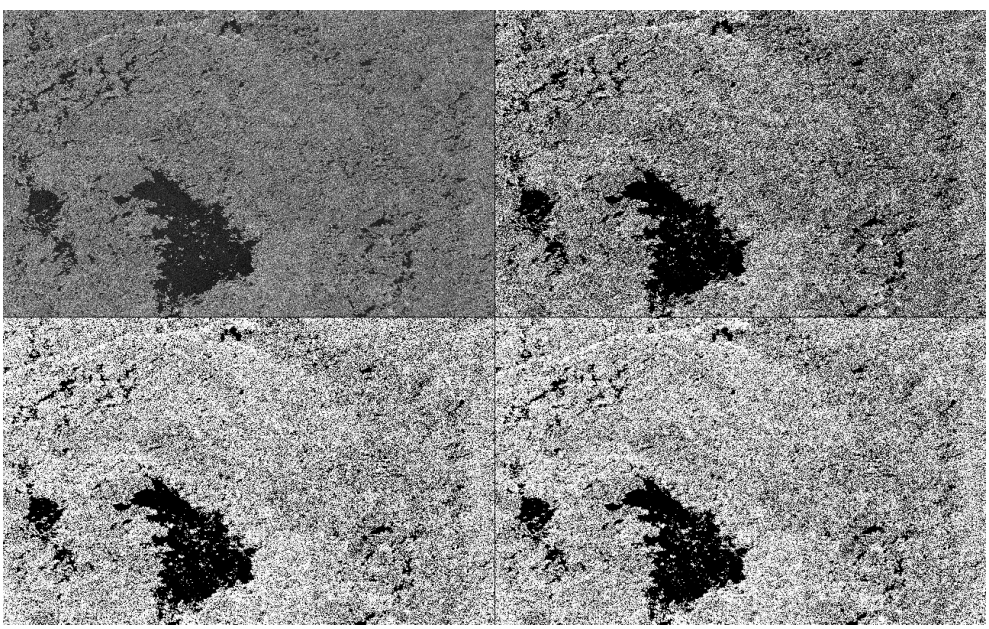

Fig. 31. Singlelook SAR image (2011. 08. 12.) and Segmentation Results

In details, the segmentation result from SAR intensity produced 40.93% as an ice concentration rate from multilook image. This result is totally different from AMSR-E data. The AMSR-E data provided 73.55% as an average ice concentration of SAR image coverage. It means underestimated value in MRF segmentation result from SAR intensity image. On the other hand, in the result from LFD, the ice concentration was 91.38% and 91.98% from the result from hybrid image. In this case, the values were looked overestimated.

For explain these discrepancy, it is natural to doubt the segmentation accuracy. For this purpose, the reference sea ice image was made as Fig. 32. The confusion matrix of this segmentation was conducted and the segmentation accuracy is given in Table. 5. By this result, the segmentation results had a trend which is similar to ice concentration trend.

The sea ice region is almost founded in the result from hybrid image. In addition, the open water region is surely founded in the result from SAR intensity image. Consequently, the segmentation results have next attributes. The result from SAR intensity has an advantage on finding open water. It can be interpreted an underestimate of sea ice region. On the other hand, the result from hybrid image shows good detection rate on sea ice region. During this segmentation, some open water regions were classified as a sea ice. By this process, the ice concentration was overestimated.

This discrepancy is originated from a characteristic of the multilook technique in SAR image processing. It makes a pixel from multiple pixels by certain calculation. During multilooking process, the melting ponds are erased and the sea ice pixels are widened. This effect is same as a blurring in poor resolution image. It would be a source of the overestimation. To avoid this effect, the singlelook image which is not suffered a multilooking procedure was used for the ice concentration calculation. In this process, the singlelook image was made from a partial region of the original SAR image due to the calculation cost.

Fig. 32. Reference Segmentation Image (2011. 08. 12.)

Table. 5. Confusion Matrix (2011. 08. 12.)

		Reference Class	
		Sea ice	Open water
SAR intensity	Sea ice	46.89	2.27
	Open water	53.11	97.73
	Accuracy		72.31
LFD	Sea ice	96.01	74.24
	Open water	3.99	25.76
	Accuracy		60.89
Hybrid (SAR+LFD)	Sea ice	99.99	51.34
	Open water	0.01	48.66
	Accuracy		74.32

(unit: %)

The partial region was cropped around the open water region like a lake shape. The partial singlelook image is presented in Fig. 31.

The segmentation results from singlelook SAR image resemble a trend in previous segmentation results. In Fig. 31 contains original singlelook image and its segmentation results. Upper left image is the partial singlelook SAR image as an original input image. Upper right image is the result from this original SAR intensity image. Lower left image is the result from LFD and lower right is from hybrid image. These results have advantage in ice concentration calculation. It reflects real aspect of the sea ice coverage on SAR image swath region.

The second estimation of the ice concentration rates are described in Table. 4 singlelook column. In this case, ice concentration rates are more reasonable than previous estimation results. The result from SAR intensity image produced 42.49% as an ice concentration. And the other results are provided around 60% ice concentration. It is consistent with the aerial photo in Fig. 27 that roughly half sea ice concentration. Moreover, it is similar to the AMSR-E result than multilook case.

To calculate the actual ice concentration, the aerial photos were selected. Fortunately, selected photos provided similar ice concentration. The actual ice concentration is regarded as 56~58%. With this result, the singlelook image is preferred for estimating the ice concentration by SAR image. The singlelook image can preserve the advantage of the high resolution image.

From above analysis, it is important that the resolution during ice concentration calculation. The passive microwave remote sensing is thought that brings an inaccurate ice concentration due to the limitation of resolution in an instrument. If it adopts more precise resolution equipment, it could give more accurate sea ice distribution and more reliable sea ice concentration. In other words, the real value of sea ice concentration is could be calculated by enough fine resolution.

Besides, the discrepancy can be evolved during the data processing. For instance, the data assimilation between different scale images could make a mismatch. Or the geo-referencing process could contain an error. Like these causes, the ice concentration values are mismatched in each data. This error is a technical issue to be resolved.

Moreover, small sea ice fragments are not exactly described in SAR image. It can be blurred by resolution limit and lose its shape especially in resampling process. This type is an error about limitation of instruments. It will be overcome by progress of engineering.

The multilooking process affects a spatial resolution. It acts reduce spatial information from raw data and reduce the speckle noise. In this manner, an analysis on the multilooking process was conducted.

First, multilooking images with various window size were made. These images were inserted in the same procedure of estimation of ice concentration. Due to the similarity between the LFD result and the hybrid result, this analysis was conducted with the segmentation results from original SAR intensity image and its LFD image.

The estimation results are presented in Fig. 33. From SAR intensity image, the larger multilook window makes the higher ice concentration. It is agreed with characteristics of multilook processing. The aim of multilook process is suppression of the speckle noise. For this goal, it sacrifices a detail of data. Therefore, the large multilook window acting as an obstacle during the segmentation with SAR intensity input.

However, in LFD calculation cases, the ice concentration values are converging to below the 60% as the window size is increasing. In addition, the convergence point is similar to the result from aerial photo case. It seems that the larger window brings more realistic segmentation results through the LFD calculation. In other words, the LFD is more accurate when using the information of wide region. Consequently, the LFD with multilook process is appropriate to the estimation of ice concentration.

This analysis supports the usefulness of LFD calculation during segmentation process. The proposed segmentation method is a good tool to detect sea ice and has robustness about the multilook process.

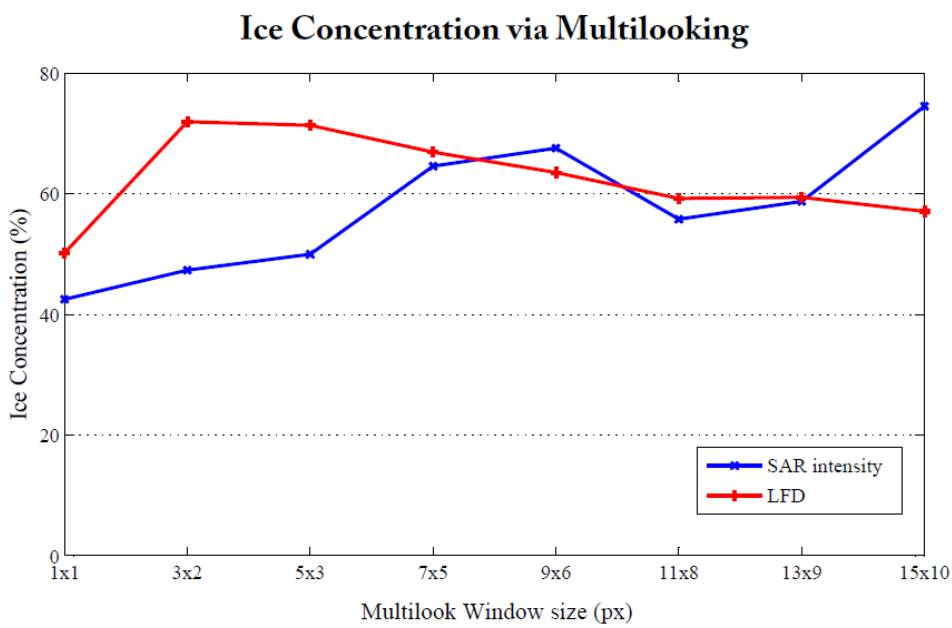

Fig. 33. Ice Concentration result from Multilook images

7. Conclusion

From now on, a new segmentation method has been proposed. It uses the characteristic of the sea ice in SAR images. The heterogeneity of sea ice from scattering mechanism is utilized for capture the property of the sea ice. With this property, the proposed method effectively detects the sea ice in SAR images. In other words, it is specialized to detect the sea ice.

The proposed method is composed with the LFD of the original SAR intensity image and the MRF segmentation method. With two ingredients, the proposed method conducts the segmentation. It enhanced the sea ice segmentation accuracy. This result is encouraging for the future segmentation developers.

In addition, the hybrid image which is combined by the original SAR intensity image and the LFD image can produce the segmentation result which is similar to the human interpretation. The reason of advance is next two statements. The LFD image helps to enhance the sea ice region. And the SAR intensity image has an advantage on detecting the open water region. Thus the hybrid image could provide a reasonable segmentation result.

With proposed method, the sea ice segmentation can be successfully performed. The proposed method brings enhanced and reliable segmentation results. These results demonstrate individual ice floes even in chaotic pattern on summer season.

In this study, the sea ice concentration rate was estimated by the segmentation results. The reasonable segmentation results provide more accurate ice concentration results rather than provided by the passive microwave sensor. The major difference between the passive and active sensor is the resolution. The passive sensor has wide swath and poor resolution. However, the active sensor can acquire fine resolution image in narrow swath width. The new ice concentration estimation is calculated from fine resolution SAR images. Thus the result in this study made a

realistic ice concentration value.

The new approach on the ice concentration is validated by in-situ based aerial photographs. It was taken by heli-borne camera system with the Korean icebreaker Araon. These photos give the actual sea ice coverage on the site. There are many melting ponds, so the sea ice coverage is roughly a half. This result is similar to the result from the singlelook SAR image. The reason is considered that the singlelook image can utilize the full information of fine resolution.

In addition, the proposed method has an advantage when the SAR image has a speckle noise. The multilook process helps the proposed method and enhances the segmentation results. So the estimation of ice concentration also is accurated.

On the contrary, the AMSR-E data is slightly over-estimated. And the multilook image based estimation was also over-estimated. In these cases, the resolution is not good as the singlelook SAR images. In multilook image, it was blurred by multilook process. The AMSR-E had a relatively poor resolution. Thus these results have some ambiguity.

By this new approach for the ice concentration will help the future sea ice researches. And it can be possible by intended satellite SAR missions. Also it can guide a technical specification of the next generation of satellite missions.

8. Future Works

The proposed method produces a suitable sea ice segmentation results from SAR images. This sea ice map is anticipated to be utilized on various categories.

First of all, segmentation results are converted an ice concentration data. Conventional ice concentration data has poor resolution. On the other hand, new approach with high resolution SAR image could produce more accurate results. The advanced result from the high-resolution SAR image based ice concentration would be a hopeful challenge. A progressing result is presented in Fig. 33. The aerial photo and high-resolution SAR image are used in this research.

In addition, the ice concentration is connected to the surface albedo. It is clear that the sea ice has a higher albedo than the open water. So the fraction of the sea ice is closely related to the albedo of the local region. In addition, the sea ice is undergone melting and broken to a small ice fragments in summer season. It hinders an estimation of the albedo. However, understanding an albedo in polar region is inevitable for the estimation of the climate system. So I want to research an algorithm for the albedo estimation. The proposed method may help this research.

Next, the sea ice segmentation results could be converted as a sea ice map. The sea ice map is useful for an iceberg tracking or ship navigation. Unfortunately, the ship navigation by polar route is not activated in this stage. However the iceberg tracking is researched from some researchers [41, 42]. By time series of sea ice images, an iceberg or an ice floe could be monitored for understanding the evolution and movement of the sea ice. Although this research is important for the interactions between the sea ice and the ocean wave and sea ice melting process investigation, the tracking algorithm still has defects.

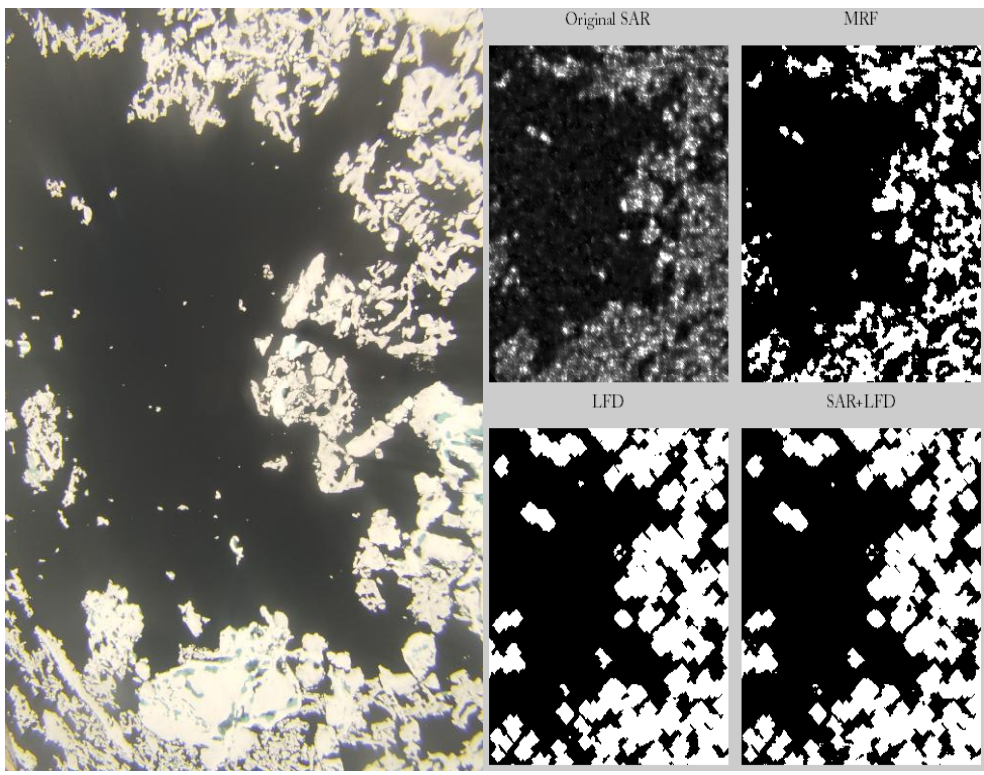

Fig. 34. Aerial Photo, SAR and Segmentation Results

The reason of hardness, the icebergs is usually transformed during their journey. So the recognition of same iceberg is sometimes failed and lost a track of the iceberg. Furthermore optic images are easily confused by covered snow. It makes a homogeneous surface and conceals the iceberg. In this manner, the proposed method may useful for iceberg tracking. It produces a reasonable sea ice segmentation result to use. With this result, it is can be investigate a tracking algorithm for iceberg detection.

And the sea ice floe analysis can be performed by proposed method. Many researchers want to know the characteristic of the sea ice. One approach contains the fractal dimension analysis on the shape of the sea ice floes. Interested variables are like that a circularity, radius-size distribution, number density and melting pond size. These variables are brought by human interpretation. However, the proposed method could provide reasonable segmentation result without human labor. In this manner, this study could be extended to the other sea ice researches. The proposed method could extract the ice floe only for analyzing the size of sea ice floe in melting season. It is anticipated on the sea ice evolution research.

Finally, this segmentation technique could be applied on the other environmental researches. For instance, the forest classification is an important mission in biomass estimation. This natural hazard map is demanded for many reasons. I anticipate these hazards have a characteristic property which is related to the LFD. If urban area is stroke by a seismic event, it will make a chaotic footprint in artificial region. It would be detected by LFD or other similar algorithm. Likewise, an oil covered area has relatively smooth surface. It also is recognized by LFD. If it is possible, the proposed method states its importance.

Reference

[1] M. Budyko and Y. S. Sedunov, "Anthropogenic climatic changes," in *Climate and Development*, ed: Springer, 1990, pp. 270-284.

[2] S. C. Moser, "Communicating climate change: history, challenges, process and future directions," *Wiley Interdisciplinary Reviews: Climate Change,* vol. 1, pp. 31-53, 2010.

[3] C. D. Thomas, A. Cameron, R. E. Green, M. Bakkenes, L. J. Beaumont, Y. C. Collingham, *et al.*, "Extinction risk from climate change," *Nature,* vol. 427, pp. 145-148, 2004.

[4] M. M. Holland and M. N. Raphael, "Twentieth century simulation of the southern hemisphere climate in coupled models. Part II: sea ice conditions and variability," *Climate dynamics,* vol. 26, pp. 229-245, 2006.

[5] X. Zhang and J. E. Walsh, "Toward a seasonally ice-covered Arctic Ocean: Scenarios from the IPCC AR4 model simulations," *Journal of Climate,* vol. 19, 2006.

[6] H. Schøyen and S. Bråthen, "The Northern Sea Route versus the Suez Canal: cases from bulk shipping," *Journal of Transport Geography,* vol. 19, pp. 977-983, 7// 2011.

[7] N. Y. Zakhvatkina, V. Y. Alexandrov, O. M. Johannessen, S. Sandven, and I. Y. Frolov, "Classification of Sea Ice Types in ENVISAT Synthetic Aperture Radar Images," *IEEE Transactions on Geoscience and Remote Sensing,* vol. 51, pp. 2587-2600, 2013.

[8] R. M. Welch, S. K. Sengupta, A. K. Goroch, P. Rabindra, N. Rangaraj, and M. S. Navar, "Polar Cloud and Surface Classification Using AVHRR Imagery: An Intercomparison of Methods," *Journal of Applied Meteorology,* vol. 31, pp. 405-420, 1992/05/01 1992.

[9] G. I. Belchansky, D. C. Douglas, V. A. Eremeev, and N. G. Platonov, "Variations in the Arctic's multiyear sea ice cover: A neural network analysis of SMMR-SSM/I data, 1979–2004," *Geophysical Research Letters,* vol. 32, 2005.

[10] J. A. Karvonen, "Baltic Sea Ice SAR segmentation and classification using modified pulse-coupled neural networks," *Ieee Transactions on Geoscience and Remote Sensing,* vol. 42, pp. 1566-1574, Jul 2004.

[11] S. Tang, P. Larouche, A. Niemi, and C. Michel, "Regional algorithms for remote-sensing estimates of total suspended matter in the Beaufort Sea," *International Journal of Remote Sensing,* vol. 34, pp. 6562-6576, 2013/10/10 2013.

[12] X. Su, H. Sang, and G. Yang, "An SVM-based method for land and sea segmentation in polarimetric SAR images," in *Image and Signal Processing (CISP), 2011 4th International Congress on*, 2011, pp. 1205-1208.

[13] P. Subashini, M. Krishnaveni, B. Ane, and D. Roller, "SVM-Based Classification for Identification of Ice Types in SAR Images Using Color Perception Phenomena," in *Innovations in Bio-inspired Computing and Applications*. vol. 237, A. Abraham, P. Krömer, and V. Snášel, Eds., ed: Springer International Publishing, 2014, pp. 285-293.

[14] H. Deng and D. A. Clausi, "Unsupervised image segmentation using a simple MRF model with a new implementation scheme," *Pattern recognition,* vol. 37, pp. 2323-2335, 2004.

[15] H. Deng and D. A. Clausi, "Unsupervised segmentation of synthetic aperture radar sea ice imagery using a novel Markov random field model," *Geoscience and Remote Sensing, IEEE Transactions on,* vol. 43, pp. 528-538, 2005.

[16] Q. Yu and D. A. Clausi, "IRGS: image segmentation using edge penalties and region growing," *Pattern Analysis and Machine Intelligence, IEEE Transactions on,* vol. 30, pp. 2126-2139, 2008.

[17] A. Qin and D. A. Clausi, "Multivariate image segmentation using semantic region growing with adaptive edge penalty," *Image Processing, IEEE Transactions on,* vol. 19, pp. 2157-2170, 2010.

[18] P. Yu, A. Qin, and D. A. Clausi, "Unsupervised polarimetric SAR image segmentation and classification using region growing with edge penalty," *Geoscience and Remote Sensing, IEEE Transactions on,* vol. 50, pp. 1302-1317, 2012.

[19] J. Sun, H.-Y. Shum, and N.-N. Zheng, "Stereo matching using belief propagation," in *Computer Vision—ECCV 2002*, ed: Springer, 2002, pp. 510-524.

[20] S. Chen, H. Tong, and C. Cattani, "Markov models for image labeling," *Mathematical Problems in Engineering,* vol. 2012, 2011.

[21] S. Geman and D. Geman, "Stochastic relaxation, Gibbs distributions, and the Bayesian restoration of images," *Pattern Analysis and Machine Intelligence, IEEE Transactions on,* pp. 721-741, 1984.

[22] F. W. Scholz, "Maximum Likelihood Estimation," in *Encyclopedia of Statistical Sciences*, ed: John Wiley & Sons, Inc., 2004.

[23] P. Kohli, M. P. Kumar, and P. H. Torr, "P3 & beyond: Solving energies with higher order cliques," in *Computer Vision and Pattern Recognition, 2007. CVPR'07. IEEE Conference on*, 2007, pp. 1-8.

[24] A. F. Silvetti and C. A. Delrieux, "Quadratic self-correlation: An improved method for computing local fractal dimension in remote sensing imagery," *Computers & Geosciences,* vol. 60, pp. 142-155, 2013.

[25] D. Guo, B. Zhang, Y. Wu, and L. Cao, "The Man-made Areas Segmentation Based on Region Growing Method Using Local Fractal Dimension," *Journal of Information & Computational Science,* vol. 10, pp. 659-667, 2013 2013.

[26] S. Novianto, Y. Suzuki, and J. Maeda, "Near optimum estimation of local fractal dimension for image segmentation," *Pattern Recognition Letters,* vol. 24, pp. 365-374, 2003.

[27] B. a. Chaudhuri and N. Sarkar, "Texture segmentation using fractal dimension," *Pattern Analysis and Machine Intelligence, IEEE Transactions on,* vol. 17, pp. 72-77, 1995.

[28] B. B. Mandelbrot, "Self-affine fractals and fractal dimension," *Physica Scripta,* vol. 32, p. 257, 1985.

[29] A. Annadhason, "Methods of fractal dimension computation," *Methods,* vol. 2, 2012.

[30] J. C. Russ, *Fractal surfaces*: Springer, 1994.

[31] C. J. Willis, J. T. Macklin, K. C. Partington, K. A. Teleki, W. G. Rees, and R. G. Williams, "Iceberg detection using ERS-1 Synthetic Aperture Radar," *International Journal of Remote Sensing,* vol. 17, pp. 1777-1795, 1996/06/01 1996.

[32] C. Rosenberger and K. Chehdi, "Genetic fusion: application to multi-components image segmentation," in *Acoustics, Speech, and Signal Processing, 2000. ICASSP'00. Proceedings. 2000 IEEE International Conference on*, 2000, pp. 2223-2226.

[33] Y. J. Zhang, "Evaluation and comparison of different segmentation algorithms," *Pattern recognition letters,* vol. 18, pp. 963-974, 1997.

[34] S. Chabrier, B. Emile, C. Rosenberger, and H. Laurent, "Unsupervised performance evaluation of image segmentation," *EURASIP Journal on Applied Signal Processing,* vol. 2006, pp. 217-217, 2006.

[35] H. Zhang, J. E. Fritts, and S. A. Goldman, "Image segmentation evaluation: A survey of unsupervised methods," *computer vision and image understanding,* vol. 110, pp. 260-280, 2008.

[36] T. Markus and D. J. Cavalieri, "The AMSR-E NT2 sea ice concentration algorithm: Its basis and implementation," *Journal of the Remote Sensing Society of Japan,* vol. 29, 2009.

[37] T. Markus and D. J. Cavalieri, "An enhancement of the NASA Team sea ice algorithm," *Geoscience and Remote Sensing, IEEE Transactions on,* vol. 38, pp. 1387-1398, 2000.

[38] S. Andersen, R. Tonboe, L. Kaleschke, G. Heygster, and L. T. Pedersen, "Intercomparison of passive microwave sea ice concentration retrievals over the high-concentration Arctic sea ice," *Journal of Geophysical Research: Oceans (1978–2012),* vol. 112, 2007.

[39] E. Center, "Sea ice concentrations from Nimbus-7 SMMR and DMSP SSM/I passive microwave data," 1996.

[40] D. Perovich, W. Tucker, and K. Ligett, "Aerial observations of the evolution of ice surface conditions during summer," *Journal of Geophysical Research: Oceans (1978–2012),* vol. 107, pp. SHE 24-1-SHE 24-14, 2002.

[41] J. Ballantyne and D. G. Long, "A multidecadal study of the number of Antarctic icebergs using scatterometer data," in *Geoscience and Remote Sensing Symposium, 2002. IGARSS'02. 2002 IEEE International*, 2002, pp. 3029-3031.

[42] K. R. Arrigo, G. L. van Dijken, D. G. Ainley, M. A. Fahnestock, and T. Markus, "Ecological impact of a large Antarctic iceberg," *Geophysical Research Letters,* vol. 29, pp. 8-1-8-4, 2002.

국 문 요 약

기후변화는 널리 알려진 이슈이다. 대부분의 사람들이 기후변화의 이유와 양상에 대해 잘 알고 있으며, 특히 북극곰과 녹아 내리는 해빙의 모습을 기후변화의 증거로서 쉽게 떠올리고 있다. 이러한 기후변화는 예상치 못한 재난을 불러 일으켜 사람들의 안전과 생활을 위협하고 있다. 특히 최근에는 기후변화의 양상이 더 급격히 진행되고 있으며, 이로 인해 재해의 규모 또한 증가하고 있다. 이러한 재해를 막고 미래의 기후를 예측하기 위해서는 기후모델에 대한 연구가 필수적이다. 이를 위해 연구자들은 컴퓨터 시뮬레이션을 통해 전 지구적인 기후모델을 생성하여 연구하고 있으며, 보다 정확한 모델을 통해 향후의 기후변화를 예측하고자 힘쓰고 있다. 최근의 기후모델들은 해빙의 특징을 표현하여 보다 정확한 시뮬레이션을 하고 있다.

해빙은 실제로 극지방의 기후연구에 큰 비중을 차지한다. 먼저 해빙과 표면의 눈은 높은 반사도를 가지고 있어 태양복사에너지를 반사한다. 반대로 해양은 태양복사에너지를 보다 많이 흡수하여 지구복사에너지 수지에 영향을 준다. 또한 해빙은 해수와 대기 사이의 열교환을 방해하는 단열재 역할을 한다. 두꺼운 해빙일수록 보다 효과적인 단열재가 되므로 이러한 연구에서는 해빙의 두께를 추정하는 것이 중요한 연구가 된다. 이외에 해빙은 해수의 염분에도 영향을 미친다. 해빙은 생성시 포함한 염분을 브라인셀(염분세포)의 형태로 내부에 가지고 있다. 이 염분세포는 염도가 높아 점차 얼음을 녹이며 밑으로 이동하여 결국 해양으로 유입된다. 이후 이 해빙이 녹게 되면 담수가 바다에 투입된다. 이러한 과정을 통해 해양의 염분은 변동하고, 열염분순환이 일어나게 된다. 이처럼 해빙은 극지방의 기후에 영향을 주어 전 지구적인 기후에 영향을 준다. 이로 인해 해빙의 특성을 연구하는 것이 필요하다.

지난 수십년간 해빙을 연구하고 감시하기 위해 많은 관측이 이루어졌다. 그 중에는 합성개구레이더를 이용한 연구도 포함된다. 합성개구레이더는 지구 대기의 영향을 받지 않는 마이크로파의 주파수를 이용하여 기후의 영향을 받지 않으면서 상대적으로 넓은 지역을 한번에 관측할 수 있다는 장점을 가지고 있다. 또한 직접 신호를 쏘고 받는 능동센서이기 때문에 야간에도 관측이 가능하다. 이러한 장점은 사람이 실제로 접근하기 힘든 극지방을 관측하기에 매우 유용하다.

최근의 많은 연구 및 관측들로 인해 수많은 해빙자료들이 획득되었다. 이 같은 자료들에서 유용한 변수들을 추출하기 위한 방법의 하나로 본 연구에서는 영상분할기법에 집중하였다. 해빙은 특수한 전자기파적 산란특성을 갖기 때문에 영상 내에서 분류해 내기 힘들다. 마이크로파 주파수로 해빙을 관찰하면, 해빙의 표면이 거칠게 보인다. 이러한 표면 거칠기와 해빙의 부분적인 유전율이 균일하지 않기 때문에 합성개구레이더 영상 내의 해빙은 불균질한 모습을 나타낸다. 또한 합성개구레이더 영상의 특징인 스페클 패턴 또한 해빙의 분류를 어렵게 만드는 요인이다. 이러한 한계점들을 극복하고자 본 연구에서는 해빙의 특성을 측정하고자 하였다.

이와 관련하여 만델브로트에 의해 도입된 프랙탈 기하학을 사용하였다. 이 프랙탈 기하에서는 자연현상에서 관찰되는 불규칙성이나 자기복제성을 표현하기에 유용하다. 이를 국소 영역에 적용하여 국소 프랙탈 차원의 개념을 사용하였다. 이를 통해 해빙에서 관측되는 불균질한 모습을 국소 프랙탈 차원으로 측정하였다. 국소 프랙탈 차원은 불규칙한 밝기값을 갖는 해빙지역에서는 상대적으로 높은 값을 가지고, 보다 균질한 바다 지역에서는 상대적으로 낮은 값을 갖는다. 즉, 국소 프랙탈 차원을 통해 해빙과 바다가 구분되는 것이다. 따라서 국소 프랙탈 차원은 해빙 분할 기법에 유용한 방법이라 생각된다.

본 연구에서는 이에 더해 마코프 랜덤 필드 (MRF) 를 이용한 영상분할기법을 사용하였다. MRF 분할기법은 마코프 확률 모델에 근거하여

통계적인 변수들을 사용하여 분류하는 기법이다. 이 때 영상 내의 화소들이 가우시안 분포를 따른다고 보고, 가우시안 최대우도함수를 이용하여 각 화소들이 각 등급에 포함될 확률을 계산한다. 또한 MRF 분류기법은 국소 화소들 사이의 관계를 이용하여 구성을 정의한다. 이 두 가지 방법을 통해 비용함수를 구성하고, 이를 최적화 계산방법 중 하나인 EM 알고리즘을 사용하여 영상분할을 수행한다.

본 연구에서 제안하는 영상분할기법은 합성개구레이더 영상에서 획득한 국소 프랙탈 차원을 MRF 모델 기반 영상분할기법을 통해 해빙을 분할하는 방법이다. 또한 비교를 위해 합성개구레이더 영상과 국소 프랙탈 차원을 합한 혼합영상을 제작하여 동일하게 MRF 모델 기반 영상분할기법을 적용하였다. 이를 통해 획득한 분할영상은 무감독 평가방법을 통해 분할 결과를 평가하였다.

본 연구에 사용한 영상은 TerraSAR-X 위성으로 촬영한 북극해의 영상으로, 주로 여름철의 해빙들이 찍힌 영상을 사용하였다. 여름에는 해빙이 녹기 때문에 합성개구레이더 영상에서 복잡하게 표현된다. 본 연구에서 제시된 방법은 기존의 분할기법에 비해 보다 개선된 분할결과를 내주었다. 분할된 영상에서 해빙의 밀집도를 추출해 내는 연구도 수행되었다. 해빙 밀집도 결과를 비교하기 위해 수동센서를 사용한 AMSR-E 영상과 항공사진을 사용하였다.

본 연구에서는 제시한 해빙 분할 기법을 통해 합성개구레이더 영상에서 해빙을 분류하여 보았다. 국소 프랙탈 차원이 해빙의 특성을 잘 포착하여 영상내의 해빙과 바다를 화소별로 잘 구분했고, 이를 이용하여 수행한 MRF 영상분할기법은 기존의 해빙분할기법보다 발전된 결과를 산출하였다. 특히 혼합영상을 통해 얻은 결과는 사람이 해석한 분류결과와 비슷했다. 그리고 분할결과를 이용하여 해빙의 밀집도도 추측해 낼 수 있었다. 고해상도 합성개구레이더를 통해 얻은 해빙 밀집도는 기존의 수동센서를 이용한 결과보다 현실을 더 잘 반영하는 것으로 보인다. 제시된 기법을 이용하여 향후 다양한 해빙의 특성을 추출하는 연구가 가능

하리라 생각되고, 여름철 북극해의 정확한 표면 반사도를 구하는 연구에도 활용할 수 있을 것으로 기대된다.

주요어 : 해빙 분류 기법, MRF 분류기법, 국소 프랙탈 차원, 합성개구레이더